Hannah Buyer, B.Sc

Assessment of new materials with high durability in sewer systems with microbial induced corrosion

MASTER THESIS

In partial fulfillment of the requirements for M.Sc. degree

in Earth Sciences

submitted to

Technical University of Graz

Supervisor:

Mag. rer. nat. Dr. rer. nat. Florian Mittermayr

Institute of Technology and Testing of Building Materials

M.Sc. B.Sc. Cyrill Grengg

Institute of Applied Geosciences

Prof. Dr. Dipl. Min. Martin Dietzel

Institute of Applied Geosciences

Graz, Juli 2017

Affidavit

I declare that I have authored this thesis independently, that I have not used other than the declared sources/resources and that I have explicitly indicated all material which has been quoted either literally or by content from the used sources. The text document uploaded to TUGRAZonline is identical to the present master's thesis dissertation.

---------- ----------
(date) (signature)

Acknowledgements

First of all, I want to thank my supervisors Florian Mittermayr, Cyrill Grengg and Martin Dietzel, and the laboratory staff at the Institute for Applied Geosciences, TU Graz for their great support. Tested samples were casted and supplied by Neven Ukrainczyk, Institue for Materials in Construction, TU Darmstadt. The microbiological analyses were carried out by Günther Koraimann and Sarah Pycha at the Institute for Microbiology, University of Graz. Special thanks to Peter Rappold and the Department of Water Resources Management, Styria, as well as to Heinz Lackner and the Department of Energy, Residential Constructions and Technology, Styria, for their financial support. Thanks to Dietmar Klammer for his efforts regarding formal implementation of this thesis.

Abstract

In this master thesis, the durability performance of alternative concrete materials exposed at two Austrian sewer systems with significant H_2S concentration and obviously deteriorated concrete walls due to microbial induced concrete corrosion (MICC) is elucidated. A multidisciplinary approach was used to evaluate newly designed geopolymer concretes (GPC) and calcium aluminate cement (CAC) mortar in comparison to two ordinary Portland cement (OPC) based materials according to ÖNORM B 4710-1. The investigations included mineralogical, geochemical and microbiological methods. This thesis comprises the mineralogical and geochemical aspects, while the microbiological findings are discussed separately in the master thesis of Sarah Pycha (Institute of Microbiology, University of Graz). The tested GPCs were manufactured using metakaolin (Metaver®R and PowerPozz™white by Newchem) based geopolymer binder (GPB) of different mix designs, casted and supplied by Dr. Neven Ukrainczyk (Institute for Materials in Construction, TU Darmstadt). The estimated total duration of the testing campaign is planned for 18 months. In this study, the materials are investigated after the first 3 months and partially after 6 months. After 6 months, all GPC showed significantly higher performance compared to the OPC and CAC. Although all samples exhibited a strong decrease in surface pH (2.4 to 4.7 pH units), no or little microstructural damage could be found on most of the GPC, while severe microstructural damages were obvious on the OPC and CAC specimen. There, intensive mineral neo-formation in form of gypsum, which was accompanied by an increase in volume has led to cracking and loss on internal strength, confirmed by severe weight gain (2.0 to 2.7 g). The calcium-free (< 1 wt. %) GPC displayed elemental sulfur as the only alteration product. However, no structural damaging could be observed. The drop of the surface pH of the GPC was attributed to leaching of alkaline cations such as sodium and potassium. The antimicrobial effect of copper sulfate in the GPC was verified by reduction of bacterial cell number (≈ 90 % in comparison to the other GPC) on the sample surface. Though, high concentrations of metal sulfates have turned out to destabilize the GP structure and promote a sudden drop of pH and structural damaging by the formation of potassium sulfate. Currently, the Power™Pozz white based GPC displayed the best performance and suggest their application in MICC systems. Further development of GPC with even more resistance against MICC should be conducted by optimizing mix design and curing conditions.

Kurzfassung

Diese Masterarbeit untersucht die Beständigkeit von alternativen Bindemitteln in zwei österreichischen Abwassersystemen mit hohen H_2S Konzentrationen und stark korrodierten Betonwänden auf Grund biogener Schwefelsäurekorrosion (MICC). Für die Untersuchung wurde ein interdisziplinärer Ansatz, d.h. mineralogische, geochemische, und mikrobiologische Untersuchungen, zur Bewertung neu entwickelter Geopolymer-Mörtel (GPC) Mischungen sowie Calcium Aluminat Zement Mörtel (CAC) gewählt. Diese wurden mit für Abwassersysteme vorgesehenen Portlandzement basierten Betonen und Mörteln (OPC) gemäß ÖNORM B 4710-1[1] verglichen. Diese Arbeit fasst die Ergebnisse der mineralogischen und geochemischen Untersuchungen zusammen. Die Ergebnisse der mikrobiologischen Untersuchungen werden detailliert in der Masterarbeit von Sarah Pycha (Institut für Mikrobiologie, Karl-Franzens-Universität Graz), diskutiert. Die untersuchten Proben bestehen aus metakaolinbasierten GPC (Metaver®R und PowerPozz™white von Newchem) mit unterschiedlichen Mischungsverhältnissen. Die Proben wurden von Dr. Neven Ukrainczyk (Institut für Werkstoffe im Bauwesen, TU Darmstadt) entwickelt und zur Verfügung gestellt. Die gesamte Versuchsreihe dauert voraussichtlich 18 Monate. Diese Arbeit umfasst Ergebnisse nach 3 und 6 Monaten. Alle GPC zeigten nach 6 Monaten eine deutliche Korrosionsbeständigkeit im Vergleich zu OPC und CAC. Trotz einer starken pH-Reduktion (2.4 bis 4.7 pH Einheiten) an der Probenoberfläche, verursacht durch Auslaugung von Alkali Ionen, wurden nur geringe chemische und mechanische Schäden an den meisten GPC festgestellt. Im Gegensatz dazu zeigten OPC und CAC Proben verbunden mit einer starken pH-Reduktion deutliche Korrosion und z.T. starke Mineralneubildung in Form von Gips was zu Festigkeitsverlust führte. Diese Proben wiesen auch die höchste Gewichtszunahme (2.0 bis 2.7 g nach 6 Monaten) auf. Die GPC zeigten als Präzipitat elementaren Schwefel, aber keine strukturellen Schäden. Die Gewichtsentwicklung der GPC war eher negativ (+0.1 bis -1.9 g). Die antimikrobielle Wirkung von Kupfersulfat wurde durch eine deutliche Reduktion (≈ 90 % im Vergleich zu den anderen Geopolymer Mörteln) der Bakterienzahl an der Probenoberfläche nachgewiesen. Hohe Metallsulfat Konzentrationen sind jedoch ungünstig für die GP-Struktur, was durch die Bildung leichtlöslichen Kaliumsulfats zu einer stärkeren pH Abnahme und strukturellen Schäden führte. Derzeit weisen die Power™Pozz white basierten GPC die geringsten Alterationserscheinungen auf. Eine mögliche Verwendung dieser GPC in Systemen mit MICC scheint daher vielversprechend. Eine Weiterentwicklung von noch resistenteren GPC gegen MICC könnte durch Optimierungen der Mischungszusammensetzungen und der Nachbehandlungsbedingungen erfolgen.

Table of Contents

1. Introduction

1.1 Scope of the study

In chemically aggressive environments like sewer systems affected by microbial induced concrete corrosion (MICC), ordinary Portland cement (OPC) based construction materials show high potential for deterioration after a few months and failure within their operation life. While the general processes of MICC are well understood (see chapter 2), to date, no cement-based concrete exists withstanding the aggressive conditions over their entire operation life, raising the demand for alternative construction materials. The goal of this study was to evaluate the performance of alternative concrete materials such as geopolymer concretes (GPC) and calcium aluminate cements (CAC) by using a multidisciplinary approach of combined mineralogical, geochemical and microbiological analyses and contemporaneous comparison to conventional OPC based concretes according to [1]. The results of this study represent an important step towards the development of sustainable materials for MICC endangered environments.

1.2 Thesis questions and approach

The aim of this thesis was the performance evaluation of newly designed GPC using a multidisciplinary field study approach. The main questions can be described as followed:

- What are the characteristics of the best performing mortars and how could the positive features be reasonably merged together?
- Which initial phases are most reactive and form new metastable phases decreasing the strength of the material?
- Is the initial surface pH and its evolution for the material crucial or not?
- How do metal additives such as Zn and Cu affect the performance of GPC?

2. Microbial induced concrete corrosion

MICC is a chain of complex processes that is associated with hazardous H_2S gas production occurring worldwide in sewer systems [2]. Besides this socially relevant problem, also a severe economic impact is related to it [2] [3]. The process is characterized by several abiogenic and biogenic redox reactions finally forming sulfuric acid (H_2SO_4), which acts aggressive against the cement phases and carbonate aggregates of the concrete. It can potentially reduce the life span of concrete elements in sewer systems to less than a decade [2]. Figure 1 shows a 10-year-old manhole wall of a sewer system strongly deteriorated by MICC.

Figure 1: Strongly deteriorated concrete walls of a sewer system affected by MICC. The outer surface consists of a material with no internal strength which can be wiped away easily with a small spoon (detail photo bottom left).

The intensity of the process is controlled by both physical and chemical parameters of the system. Sewer systems with low flow rates or long retention times facilitate the accumulation of sediment layers and biofilms on the submerged sewer walls (Figure 3). Due to bacterial oxidation of organic matter within the biofilm, anaerobic conditions evolve. Due to this depletion of oxygen (O_2) and nitrate (NO_3^-), anaerobic reduction of sulfate (SO_4^{2-}) during the oxidation of organic carbon by different strains of sulfate reducing bacteria (SRB, e.g. *Desulfovibrio spp.*) proceeds [4] [5]. The metabolic products are sulfide species, which pH-dependent distribution is illustrated in Figure 2, as well as carbon dioxide (CO_2) and volatile organic compounds (VOCs).

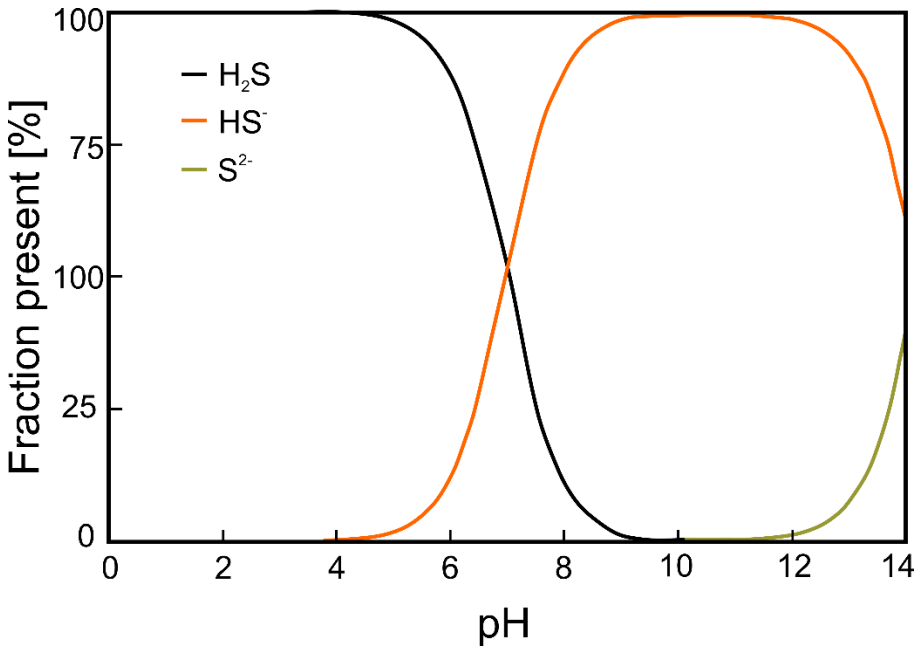

Figure 2: Distribution of the three sulfide species as a function of pH at 25°C (modified after [6]**).**

High levels in turbulence promote degassing of CO_2 and H_2S into the sewer atmosphere. Thus, transfer regions from penstocks to gravity pipes with characteristic high turbulences favor the degassing of these gases and thus the potential for the evolution of MICC. The gases produced emit into the atmosphere of the sewer systems and consequently dissolve and migrate into the humid pore network of the concrete. There, different reaction pathways (Figure 3) lead to the formation of H_2CO_3 and H_2SO_4, which react with the alkaline cement phases e.g. calcium-silicate-hydrate (C-S-H) phases and calcium hydroxide (portlandite; Port) reducing the surface pH of the concrete down to ≈ 9. After this initial abiotic pH reduction of the concrete surface, the colonization of neutrophilic sulfur oxidizing bacteria (NSOB, e.g., *T. thioparus*, *Starkeya novella*, *H. neapolitanus*) occurs [7] [8]. *T. thioparus* metabolizes thiosulfate ($S_2O_3^-$), which can be the product of abiotically oxidized sulfide at moderate

pH values, to tetrathionate ($S_4O_6^{2-}$) [8]. Further reactions of polythionic acids ($H_2S_{2+n}O_6$) reduce the pH of the concrete and promote the establishment of other species such as *T. neapolitanus* [8]. At a pH < 9, abiotic as well as biotic conversion of thiosulfate to elemental sulfur (S^0) can occur, resulting in the deposition of sulfur on the concrete surface. From pH 4.5, acidophilic sulfur oxidizing bacteria (ASOB, e.g. *A. thiooxidans, A. ferrooxidans)* and acidophilic heterotrophs begin to grow and to metabolize mainly elemental sulfur to sulfate [8]. Besides, a close association between SOB and concrete surface colonizing heterotrophic fungi is suggested by several studies [9] [10]. The isolated fungi seem to be able to oxidize sulfide species to thiosulfate ($S_2O_3^{2-}$), a form of aerobic biotic oxidation of sulfur (Figure 3), supplying an energy source for ASOB. The energy source for the fungi are organic compounds produced by the bacteria which results in a symbiotic relationship of these microorganisms. In addition, the fungi show high tolerance against acidic conditions despite their growing optimum at neutral pH [9]. Contrary to the concept that these extremely acidic environments only allow for very few species to adapt, recent studies have shown that the community of microorganisms can be diverse and adapt to the environmental conditions in the particular sewer system [11] [12] [13].

ASOB produce H_2SO_4 lowering further the pH of the concrete surface by acid-base reactions between H_2SO_4 and the cementitious phases and carbonic aggregates of the concrete. These processes of mineral dissolution and neo-formation are proceeding in a dynamical system, mainly controlled by pH and diffusion and associated characteristic elemental distributions. The non-corroded concrete displays a strongly alkaline pH around 13 [14], dominated by siliceous and/or carbonatic aggregates embedded in Port ($Ca(OH)_2$) and C-S-H phases of the cement matrix. Within the corrosion front, the pH of the concrete drops (possibly <1 [15]) caused by the presence of H_2SO_4 and polythionic acids. Simultaneously, the formation of sulfate phases mainly in the interfacial transition zone (ITZ), the zone between aggregates and cement matrix with high $Ca(OH)_2$ content, occurs [16]. Due to the high specific volume of these phases, crack formation in the cement matrix proceeds. Depending on the pH, also other phases (e.g. Mg-/Al- and Fe-hydroxides) are formed within the corrosion front, precipitating and dissolving in a dynamic system controlled both by pH and diffusion. This process is discussed in detail in Grengg et. al (2017, in press) [15]. Regions of heavily corroded concrete with pH < 2 are dominated by gypsum (Gp; $CaSO_4 \cdot 2H_2O$), anhydrite ($CaSO_4$) and basanite ($CaSO_4 \cdot 0.5H_2O$) as well as amorphous silica ($n.SiO_2$) [17].

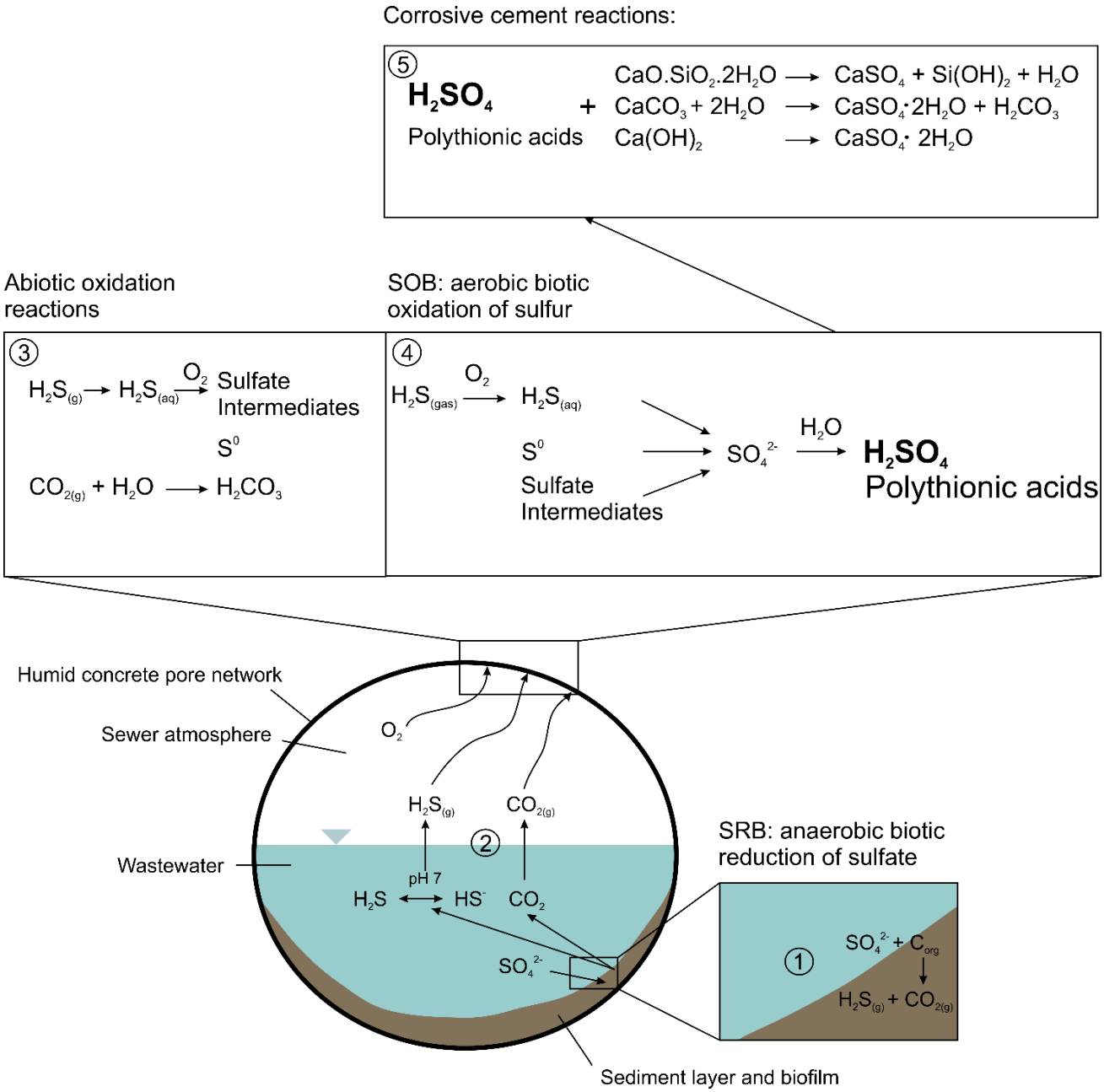

Figure 3: Schematic view of a sewer pipe cross section. Illustrated are the sulfur and carbon pathways in the sewer system. (1) The bottom right box shows processes in the submerged zone, including the anaerobic biotic reduction of sulfate adsorbed from the wastewater within the biofilm by sulfate reducing bacteria (SRB) producing thereby H_2S and CO_2. (2) Depending on the pH of the wastewater, different H_2S species are dominant and only at pH < 9, the dissolved H_2S can degas in the sewer atmosphere. (3) The two middle boxes show processes occurring in the condensate film of sewer crowns or manhole walls. The two abiotic oxidation reactions result in the formation of carbonic and sulfuric acid. (4) shows the main metabolic pathways of the aerobic oxidation of sulfur by SOB resulting in sulfuric and polythionic acid(s). These two chemical sulfur pathways are linked by the elemental sulfur molecule and different sulfate intermediates (e.g. $S_2O_3^{2-}$, $S_4O_6^{2-}$). (5) presents processes occurring in the pore network of the concrete matrix consuming the prior produced H_2SO_4/polythionic acids. The resulting product is mainly gypsum ($CaSO_4 \cdot 2H_2O$).

O'Connell et al. (2010) identified ettringite (Ett; $Ca_4Al_2(SO_4)(OH)_2H_2O$), precipitating directly at the corrosion front where the pH was higher [2]. Ett was also observed in cracks pervading into the un-corroded concrete [18] [19]. Newly formed phases such as Gp and Ett have a high specific volume and the crystallization pressure is leading to a critical stress regime in the concrete matrix which results in (micro) structural damage of the concrete [20].

First microbial analyses of deteriorated concrete exposed to gaseous H_2S were carried by Parker (1945). The study focused on acidic pH conditions (around pH 4.0) under cultivation and identified *A. thiooxidans* as the most abundant microorganism [21]. Recent studies used molecular techniques (DNA-sequencing) and were focused on the pH-dependent succession of various phylotypes of SOB [22]. The phylogenetic relatives of the bacterial community vary with time and pH from neutrophilic to acidophilic phyla as discussed in detail above [7] [22].

3. Alternative Binders

A replacement of OPC as the dominant binder in construction is far in the future, but in many applications, it is reasonable to test and apply different materials [23]. In this study, two alternative binder systems have been chosen to be tested in sewer systems affected by MICC. This chapter introduces the materials and describes potential durability performance advantages compared to OPC based materials when exposed to MICC.

3.1 Calcium Aluminate Cement

3.1.1 Introduction and state of the art

The first precursor of CAC was a product made of limestone and bauxite, patented in 1888. Industrial implementation of the idea of alumina rich cements was done by the Lafarge company at Le Teil, France [24] for the application in sulfate containing soils which have emerged to be aggressive against mortars and resulted 1918 in the product named Ciment Fondu Lafarge (CFL). The cement offered not only high sulfate resistance but also rapid hardening, heat-resistance and resistance to abrasion. Thus, the spectrum of applications in demanding environments is wide due to the high durability of CAC, e.g. for special floor tiles [25], for building materials exposed to severe bio-colonization both in marine environments [26] [27] and in sewer networks affected by MICC [28]. Nevertheless, the use of CAC is accompanied by a chemical and an economic challenge. The chemical one is called conversion which involves that at low temperatures metastable hydrates convert into stable forms accompanied by an increase in porosity and loss of strength. Yi and Thomas (2014) tested the addition of slag/silica fume with success to overcome the process of conversion [26]. The second disadvantage compared to OPC is the limited supply of bauxite and the entailing costs [29].

3.1.2 Chemical structure

The term CAC is used for types of cement which contain > 36 wt. % alumina [29]. The reactive phases are calcium aluminates (CA, $C_{12}A_7$, CA_2) which form calcium aluminate hydrates, when water is added. Small amount of silica lead to C_2S (Belite) or C_2AS (gehlenite) as major silica containing

phases. Iron oxides (ferric and ferrous compounds) vary in percentage depending on the field of application up to 20 percent [29]. The clinker phases as well as the hydration products of CAC are primarily X-ray amorphous with varying numbers of crystalline phases (e.g. gehlenite, mayenite, birnessite).

3.1.3 Advantages and application

A widespread disposition of CAC or even the replacement of traditional OPC never happened. But due to its advantages, like rapid hardening and enhanced durability in chemically aggressive environments like MICC, the application in other, non-refractory fields of construction has been intended. Furthermore, the carbon footprint of CAC production seems to be better than of OPC [23]. The application of CAC in sewer systems exposed to MICC showed consistently good results. Goyns et al. (2014) showed the significantly better performance of CAC based sewer pipelines compared to OPC based ones, stating to be at least an order of magnitude more durable [28]. This higher resistance of CAC against biogenic corrosion may be due to the higher acid neutralization capacity of $Al(OH)_3$ compared to $Ca(OH)_2$ in OPC while creating an alumina gel layer during the reaction with H_2SO_4, which remains stable down to pH 4. The precipitation of the alumina gel reduces the surface porosity and thus the percolation of H_2S as well as a biofilm adhesion [30]. The bacteriostatic effect of aluminum as stated in some studies [31] [32] has recently been questioned by other studies [33] [34]. Nevertheless, CAC have shown a better performance compared to OPC in MICC environments and thus have already been used as sewer pipe coatings or for repair measures.

3.2 Geopolymer Binder

3.2.1 Introduction and state of the art

Early scientific ambitions to replace OPC by alternative binders as a construction material occurred in the first half of the twentieth century. Inspired by natural zeolites forming in deposited volcanic rocks at low temperatures, scientists investigated alkaline alumo-silicate cement systems [35] [36] [37]. The technology exploited the rapid hardening of a slag cement mixture by adding NaCl and NaOH [38]. In the early 1970’s, the French scientist Joseph Davidovits, introduced a different approach for the development of new inorganic binders. It was based on the synthesis of hydrosodalite

from kaolinite at 100° C in concentrated caustic soda (NaOH). The term *geopolymer* evolved in 1979 describing inorganic polymeric alkali-alumo-silicates [39]. This first scientific research focused on the development of new heat-resistant materials replacing organic resins [40]. The synthesis of organic polymers under hydrothermal (< 150° C) conditions, high pH-values and concentrated alkalis was adapted to inorganic materials to develop a geopolymer binder system that hardens at room temperature with similar physiochemical properties as OPC based concretes [39]. Such inorganic alkali-alumo-silicates have already been synthetized in the 1950's in form of zeolites as molecular sieves [41]. But for the development of innovative alternative binders, the technology was new [42]. First mixtures, composed of kaolinite from clay and caustic soda (NaOH), poly-condensed at 100 to 150° C and formed three-dimensional silico-aluminate materials. These geopolymer gels hardened rapidly at room temperature. A further stage of the synthesis was reached, when dehydrated, highly reactive kaolinite (metakaolin; dehydration at ~550°C) was used in combination with soluble alkali silicate (Na-silicate in this case) as raw materials. The main advantages of this technology were the reduced demand on mineral binder as well as the low production temperatures (highest needed temperature ~550°C to obtain metakaolin from common clay). In 1983, early high-strength geopolymer cements were introduced and patented in 1985. By now, a broad selection of raw materials for geopolymer cement has been tested (e.g. fly-ash, slag, calcined clay, alumo-silicate powders and natural minerals) and many geopolymer binder systems have been created (partly patented) [38] [43] [44]. Despite this broad academic and scientific interest in geopolymer binders, there is no significant commercial establishment [45]. The current challenge is to reproduce well-performing mixtures with good workability in a commercial form for a broad field of applications.

3.2.2 Chemical structure and terminology

The main compounds of geopolymer binder (GPB) are alumina silicate materials (calcined clays, volcanic rocks, blast furnace slag, fly ash), mixed with an alkaline reagent solution, e.g. sodium or potassium soluble silicates and water to form a cage-like structure when setting at room temperature [42]. GPC is prepared by mixing GPB with fine aggregates like quartz sand. The chemical structure of all geopolymeric materials are AlO_4^{5-} and SiO_4^{4-} tetrahedrons, linked by an oxygen in a covalent bond, namely an ortho-sialate molecule. Charge balance of the tetrahedral aluminum is achieved by alkali cations (mainly K^+ from KOH or Na^+ from NaOH) incorporated in the alumo-silica framework. The polymerization process involves 3 phases:

(i) The alkalination, where alkaline depolymerization of the poly-(siloxo) layer of kaolinite or another raw material proceeds together with the formation of highly reactive tetravalent Al-side groups due to the reaction with the alkaline solutions (KOH, NaOH). Additionally, the primary unit forms due to the ordering of Si-OH groups, which react later with Na^+/K^+ to reactive Si-ONa/Si-OK-groups.

(ii) The gelation comprising the formation of the monomeric ortho-sialate (OH_3) Si-OH-Al-$(OH)_3$ molecule and consequently the first setting of the mixture.

(iii) The last step is the polymerization, which comprises the condensation of dimers into higher oligomers and polymers resulting in the hardening of the material. It starts with two linked siloxo/sialate tetrahedrons (di-siloxonate) and proceeds to polymeric siloxonates by sharing electrons of the silicon and oxygen.

The microstructure of fully reacted, amorphous regions of the GP matrix is composed of nano-sized (5 to 20 nm) aluminosilicate-assemblies which form channels and pores resulting in a 3D-network with a nanoporosity of 3 to 10 nm [46] [47]. This reaction process has been modelled by Provis and Deventer (2007) [48]. The eventually built crystalline components of a geopolymer gel, maintained warm and sealed, are described as mainly zeolites of simple structure, like sodalite, faujasite, gismondine and Linde Typ A frameworks [49].

Geopolymers can be classified by their initial Si : Al ratio, which is determined by the used raw material and mix design. For the GPB, characteristic classes derived from the their raw material are common [4].

3.2.3 Advantages and application

The performance of GPC has been tested in different applications. Concerning physical properties and constructional applications, GPC perform equivalent or even better in acidic and chemical aggressive environments compared to OPC [39] [50]. This is due to the high reactivity (solubility) of calcium-rich phases present in OPC, which dissolve in acidic conditions. Hence, GPC show an overall advantage of the chemical structure. Compared to OPC the geopolymer structure is less reactive in acidic environments. The chemical structure is a 3D-network of almost calcium-free alumo-silicates. This alumo-silicate network shows high stability between pH 11 and 4, whereas $Ca(OH)_2$ is reacting immediately with a weak acid (e.g. H_2CO_3). The Port crystals in OPC form a porous and mechanically

weak zone around the aggregates – the ITZ – and make OPC physically and chemically even more vulnerable than GPC [51]. GPC exhibit a dense microstructure with no weak zones around aggregates. If there is no excess of alkali metals in the geopolymer binder matrix, the carbonation process does not form high soluble carbonates weakening the structure [18]. Therefore, the degree of polymerization is essential regarding the structural and chemical durability of the material. Alkali metals bound in the GP matrix display a high buffer capacity and prevent a sudden drop of the pH under acidic conditions [52]. Cyr and Pouhet (2016) [53] showed that under atmospheric CO_2 conditions the surface pH of GPC is constant at 10.5 over one year which means there arises no risk of corrosion by carbonation, what makes GPC suitable for the application in reinforced concrete. The compressive strength of the GPC was also stable over the test period, although the formation of efflorescence seems to be a common problem [54] [55]. The performance of GPC under influence of a 5 % H_2SO_4 solution showed a weight loss of < 10 % after 28 days at room temperature in comparison to a weight loss of OPC of > 90 % and CAC of > 40 % [39]. The positive behavior of GPC under these conditions suggests a positive performance in acidic environments. As the immersion of concrete specimen in liquid acids does not represent the process of acid attack in MICC environments, the performance of GPC in systems with high H_2S concentration has to be evaluated in-situ.

The use of GPC instead of OPC has also a positive ecologic impact. The issue is to use materials without calcium-based cements and a decreased need of carbon-fuel combustion during the production process [13]. The production of GP requires less energy and generates less CO_2. At the best, the production of GPC can be achieved exclusively with industrial waste materials. Fly ash and slag have turned out to improve the workability, combined with a lower water demand compared to metakaolin based GPB [56].

4. Field Study and Experimental Approach

Different mortars and concretes, including 9 GPB mixtures (with and without metal (Cu/Zn) additives), one CAC, one OPC based mortar and one OPC based concrete were tested regarding their performance in two different sewer systems strongly affected by MICC. The mortar samples were casted and supplied by Dr. Neven Ukrainczyk (TU Darmstadt, Institute for Materials in Construction). Additionally, a reference sample of conventional high acid resistance concrete suitable for aggressive conditions in sewer systems according to standard regulation OENORM B 4710-1 [1] was tested. The duration of the in-situ tests is still ongoing and will last up to 18 months. This thesis comprises sampling and examination of samples stored 3 months and selected samples after 6 months. Sarah Pycha and Prof. Günther Koraimann (University of Graz, Institute for Microbiology) conducted the microbiological sampling (see [57])

4.1 Pastes and mortar samples

In the laboratory examined samples include the raw materials (see table 1; MW0, PP0, TRASS, PC0, CAC0), used for the mix design, as well as the pastes of the in situ tested mortar samples. All tested mortars are designed with one or two of the following raw materials, listed in Table 1.

Table 1: Raw materials

Product	Description	Paste Sample
Metaver®R (Newchem)	Calcined kaolin (metakaolin +Qz); Pozzolanic hardening additive	MW0
PowerPozz™ white (Newchem)	Calcined, ultra-pure kaolin (metakaolin); Pozzolanic hardening additive	PP0
Trass (tubag)	Pozzolanic tuff	TRASS
Sulfo 5 R (Holcim AG)	Portland cement CEM I 52.5 R-SR3/NA (2) after DIN 1164-10. with high sulfate resistance	PC0
HiPerCem® CAC 50 (Calucem)	Calcium Aluminate Cement	CAC0
Geosil	Potassium silicate solution	Not evaluated
Normensand	Quartz-dominated sand	Not evaluated

All GPBs are Metaver®R (MW0) or PowerPozz™ white (PP0) based and reacted with a potassium based silicate solution (GEOSIL), including 5 GPB with metal additives. The metabolism of all microorganisms might be influenced by metals as e.g. copper [58], arsenic and zinc [59] [60]. However,

the toxicity to microorganisms depends on many factors, like on the growing conditions and the adaptability of the microorganisms to specific element concentrations. In this master thesis, the impact of copper and zinc was studied. Table 2 explains all tested mortar samples including the reference concrete B6. Table 3 shows the detailed mix design of all tested mortars.

Table 2: Overview of the tested mortars and concrete.

Mortar [Paste with Qtz-sand aggregate]/ Concrete	**Containing paste(s)**	**Description and raw materials**
GP_PP	PP0	PP0 based geopolymer.
GP_PPT	PPT	Mixture of PP0 and TRASS.
CAC	CAC0	Hydrated CAC0 paste, containing mainly calcium aluminate hydrate phases.
GP_MK1	MK1	MW0 based geopolymer.
PC	PC0	Hydrated PC0 paste, containing mainly C-S-H phases.
GP_MK2	MK2	MW0 based GPB.
GP_Zn1	Zn1	MW0 based GPB with $ZnSO_4$ additive.
GP_OZn1	OZn1	MW0 based GPB with ZnO additive.
GP_OZn2	OZn2	-“-.
GP_Cu1	Cu1	MW0 based GPB with $CuSO_4$ additive.
GP_Cu2	Cu2	-“-.
B6	-	C_3A free CEM I (SR0); chemical exposure class acc. ÖN B4710-1 XA2L/XA2T

Table 3: Mix design of all mortars except for the B6 concrete. All values are given in [g].

Sample	Water	CEM I	CAC	Geosil	PowerPozz-™white	Trass	Metaver®R	Sand	$MeSO_4 \cdot H_2O$ /ZnO
GP_PP				475	450			1350	
GP_PPT				404	315	135		1350	
CAC	225		450					1350	
GP_MK1				356			450	1350	
PC	225	450						1350	
GP_MK2				425			400	1350	
GP_Zn1				425			400	1350	21.99
GP_OZn1				425			400	1350	6.22
GP_OZn2				425			400	1350	12.45
GP_Cu1				425			400	1350	18.93
GP_Cu2				425			400	1350	37.86

4.2 Study site and sampling

For obtaining the durability of the introduced mortars/concretes in sewer systems, two locations were chosen. Both systems are located in the North of Graz (Styria, Austria) and showed an evident corrosion due to the prevailing H_2S concentration in the sewer atmosphere. In the first location (called "system I"), prismatic (ca. 8 x 4 x 4 cm^3 and average weight of 260 g) samples were fixed on the manhole cover with a wire having no contact to the liquid phase of the system with except of dripping water. In the second location ("system II"), the samples were placed in plastic boxes with perforated bottoms on a platform (see Figure 4).

Figure 4: Sample preparation and placing in both systems. In system I, all samples are wire-fixed on the metal inlay beneath the manhole cover. The samples in system II are placed in perforated boxes on an elevated platform. Note the heavily corroded concrete walls of this sewer system. The mushy material on the bottom illustrates the severe deterioration.

4.3 Methodology

4.3.1 On-site monitoring of the sewer systems

Over parts of the sampling period, relative humidity (RH) was measured by a humidity logger. For the monitoring of the variability in the H_2S concentration and temperature (T), in both systems a long-term gas and temperature measurement myDataSens1000 H_2S gas monitor was installed.

4.3.2 Material characterization

Surface-pH, weight and photo documentation

To record the corrosion process of the mortar samples, a photo documentation of all prisms was conducted. Initial weight and surface pH (at least 4 spots/sample) were measured on mortar samples dried at 40° C for 24 h. After 3(6) months, the samples were weighed again after drying at 40° C for 24 h. To determine the surface acidity, the ExStik® pH- Meter Extech PH100 (Extech Instruments by FLIR Systems, Inc.) with an internal error of ± 0.01 (as specified by the manufacturer) was used. The variance of the measurements scattered between ± 0.07 and ± 0.90. On at least four of six surfaces of each sample, pH point analyses were conducted and averaged per sample. The surface was damped with two drops of ultrapure water to apply the pH probe. After about one minute, the equilibrated value was noted. The pH measurements after 3 and 6 months were conducted using an optical chemical sensor with a precision of ± 0.01. The scattering of the measured values was due to different surface conditions after the alteration (range between ± 0.03 and ± 1.48). The measurement set-up consisted of pH-sensitive dyes with characteristic pKa values. This principle is based on pH sensitive photo-induced electron transfer between the used dye and an amine. For the radiometric measurement of the pH, the phase angle of the shift between the dye and a phosphorescent reference dye is measured and corresponds to a single pH-value. This method is called dual lifetime referencing (DLR) [61] [62] and is advantageous in comparison to common surface measurements due to better spatial resolution, a more precise calibration and less disturbance by damping water. As a consequence, DLR does not show deviations in high acidic and high alkaline pH ranges.

Solid phase analysis

X-ray powder diffraction (XRD) was performed to determine the initial phase composition of the samples, the raw materials as well as the paste mixtures. For this purpose, a representative quantity of the initial material was powdered using an agate-mortar. To analyze quantitative phase proportions with XRD analysis, the particle size should not exceed 5 μm [63]. Hence, the samples were grounded in a McCrone Micronizing Mill (McCrone Microscopes & Accessories) after adding 10 wt. % ZnO as internal standard (only for the unaltered paste samples). Ethanol was used as grinding liquid and with a fixed grinding time of 8 minutes. Finally, the samples were dried at 40 °C for 48 h and front loaded into the sample holder for analyzing randomly oriented samples. The same method was used to detect phase changes after 3 and 6 months exposure time. In this case, no grinding was necessary. The powder samples of the outermost surface, which was exposed to the sewer atmosphere, were prepared with a Dremel® drilling machine and then analyzed. For the measurement, a PANalytical X'Pert PRO X-ray Powder Diffractometer equipped with a Co-tube (40 kV and 40 mA), a rotating sample stage, 0.5° divergence and anti-scattering slit and a Scientific X'Celerator detector. The scan was run from 4 to 85 [°2Th.] with a step size of 0.0080 [2°Th.] and a count time of 40 s/step. For the phase identification, the experimental XRD data was compared to reference patterns of the databases using HighScorePlus, v.2.2e (PANalytical). For the further treatment, the background (amorphous phases) was not subtracted.

Major and trace element analysis

Wave-length dispersive X-ray fluorescence analysis (XRF) was performed to investigate major and trace elements of the pastes. To determine main and trace elements of the unaltered pastes (raw materials and mixtures), the pastes were grinded in an automatic agate mortar for 10 minutes to reach a fineness of about 10 μm. The trace element analysis was performed on non-annealed samples (dried at 105 °C for 24 h). For this, about 4 g sample aliquot was pressed with a cylinder type die at 20 MPa for 20 seconds using Hoechst wax C micro powder (0.2 %) as tableting aid. To carry out the main element analysis on glass pellets, samples were first annealed in the muffle kiln for 1 hour at 950 °C. About 1 g sample aliquot (samples with trace metals about 0.05-0.1 g) were further grinded together with the mixture $Li_2B_4O_7$ LiB_2 (86 %) as flux to prepare them for the fusion bead method using a Perl'X3 Automatic Bead Machine (1050 °C for 10 minutes). For the measurements, a PANalytical 2404 X-ray fluorescence vacuum spectrometer, equipped with a PW2540 X-Y sample handler and a

4 kW Rh super sharp X-ray tube, was used. The evaluation of the trace elements was performed with the program ProTrace (PANalytical), of the main elements with the software SuperQ (PANalytical).

Microscopic surface

To investigate the surface of all deteriorated samples, a VHX-5000 digital microscope (Keyence Corp.) was used. From all surfaces, which underwent the epifluorescence method, panorama views at a 20 x magnification were photographed. Additionally, noticeable regions and pores with obviously mineral precipitation were photographed at a 200 x magnification. A selection of these detailed pictures is located in chapter 5 (“Results”) under the subitem “Microscope”, the rest can be found in the Appendix A-1 (chapter 9.1).

4.3.3 Microbiological analysis

Epifluorescence

To visualize bacterial growth in form of DNA or RNA throughout the deteriorated samples a mixture of SYTO® 9 (green fluorescence) with propidium iodide PI (red fluorescence) which show fluorescence in presence of living as well as dead DNA/RNA was used. For detecting the fluorescent signals blue or green excitation LEDs together with fluorescein or rhodamine filters and a ChemiDoc MP (BioRad) imaging system was used. The sample preparation and analysis was made at the Institute for Microbiology (more detailed information will be given in the Master Thesis of Sarah Pycha [57]).

5. Results

5.1 On-site monitoring of the sewer systems

The progression of the H_2S gas concentrations for both systems as well as the temperature during the sampling period are shown in Figure 5. The data of system I provided by the long-term gas monitoring of VTA Technology GmbH, showed an average concentration of ~13 ppm H_2S gas and a variation between 0 and 103 ppm. System II exhibited an average gas concentration of ~12 ppm with a maximum of 333 ppm. Hence, the average H_2S concentration of the two systems was nearly the same.

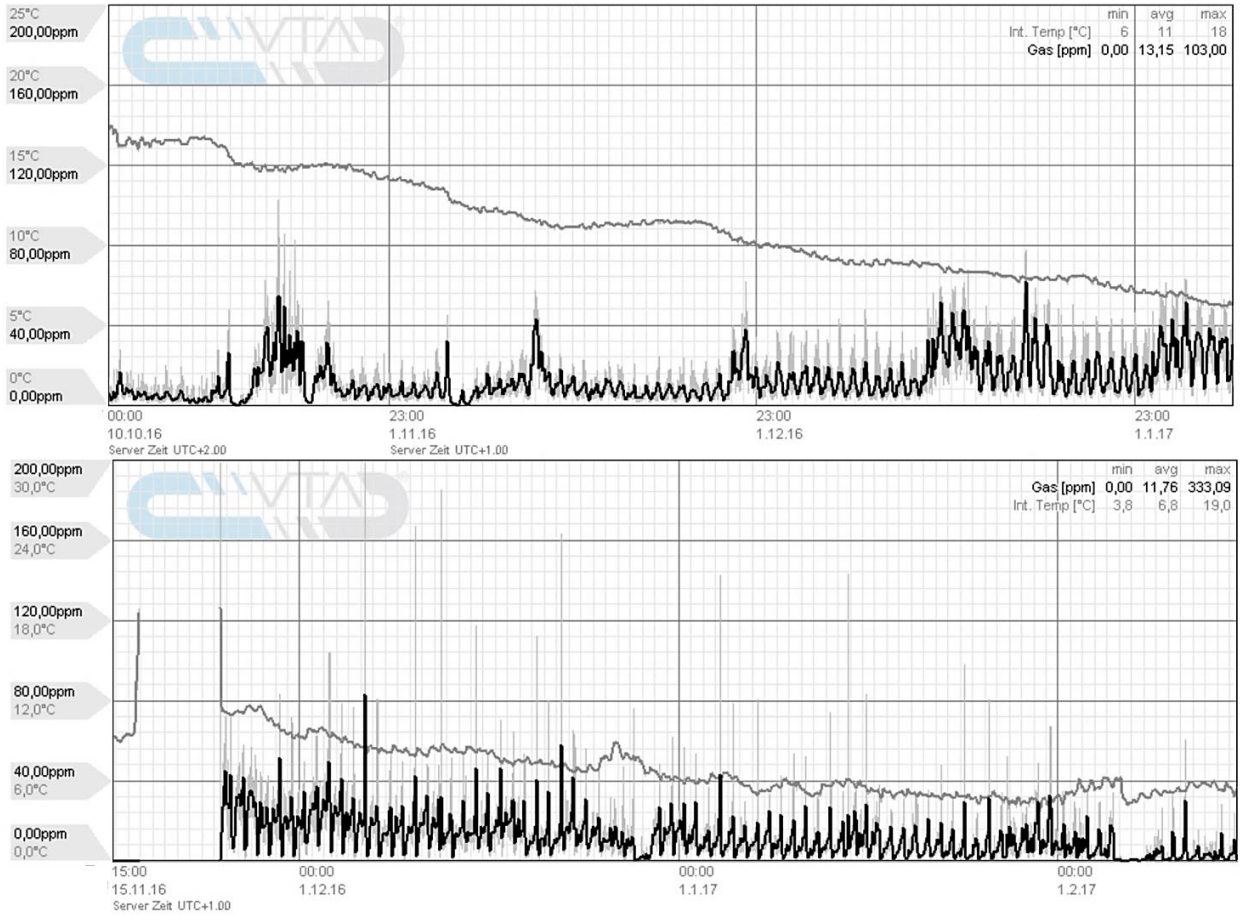

Figure 5: Evolution of the H_2S gas concentration in system I (on top) and system II (below) during the first 3 months of the test period. The x-axes are labelled with the time, the y-axes with the gas concentration in ppm. The dark grey line displays the temperature, the light grey line is the maximum H_2S concentrations. The periodicity of the peaks matches with pumping cycles.

However, system II showed higher peak values than system I. In system II, a typical seasonal, temperature-affected variation of the gas concentration occurred, where the gas concentration decreases

with temperature. System I displayed the opposite trend of increasing peak intensity with falling temperature.

The relative humidity [%RH] in system I (Figure 6) displayed variations between 17 % RH and 103 % RH (average 58 % RH) in system II (Figure 7) between 69 % RH and 95 % RH (average 79 % RH). The daytime oscillation could be associated to the temperature/insolation and was much higher for system I, which had also the lower average humidity. Additionally, a seasonally decrease of the relative humidity during spring could be seen.

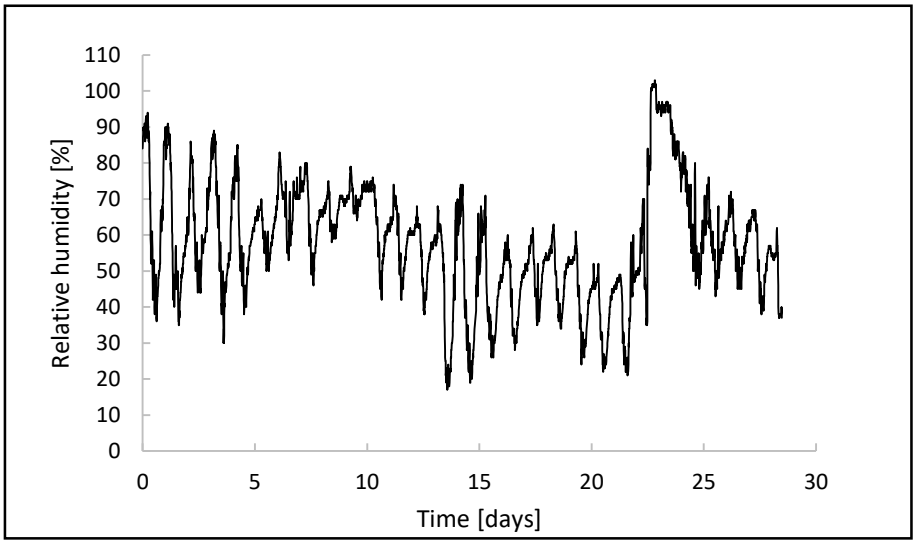

Figure 6: Evolution of the relative humidity in system I within 28 days (13.03.2017 to 10.04.2017).

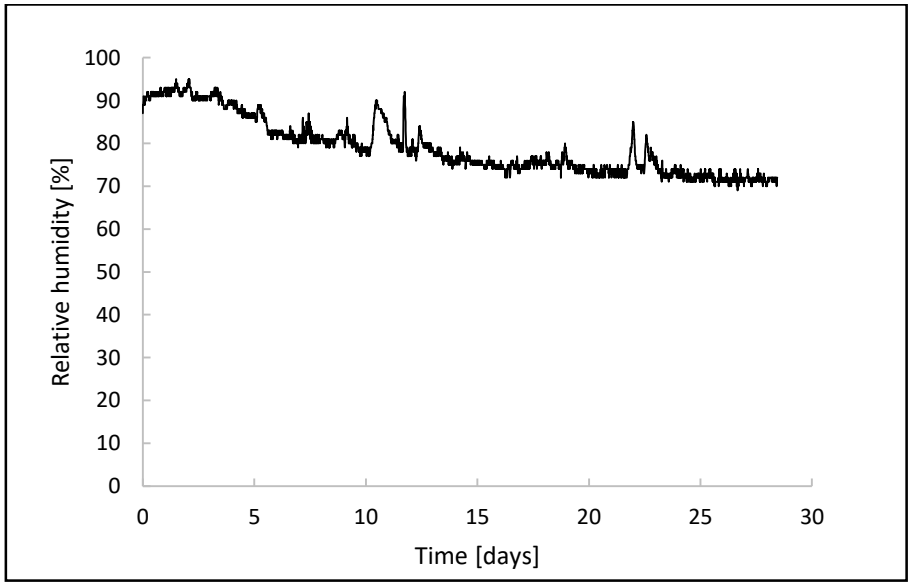

Figure 7: Evolution of the relative humidity in system II from within 28 days (02.05.2017 to 30.05.2017)

5.2 Material characterization

Initial material

The results of the initial surface pH and weight measurement are listed together with all measured values after 3 and 6 months in Table 6 and Table 7.

The chemical composition of the raw materials, the pastes and the concrete was determined by XRF and is shown in Table 4 and Table 5. All elements are given as oxides, except for the trace metals Zn and Cu. The unit is weight percentage [wt. %]. The table only refers to values > 0.1 %. All raw materials for the GPB mix design (Table 4) were dominated by aluminum and silicon, TRASS exhibited more trace elements, as well as more alkali metals and Fe_2O_3 than PP0 and MW0.

Table 4: Chemical composition in weight percentage [wt. %] of the raw materials used for mixtures. All raw materials were dominated by silicon and aluminum.

Paste	Na_2O	MgO	Al_2O_3	SiO_2	SO_3	K_2O	CaO	TiO_2	Fe_2O_3	P_2O_5
MW0		0.3	22.0	66.8		0.4	2.0	1.0	4.2	
PP0	0.1		39.9	55.7		0.3		1.4	1.8	
TRASS	3.0	1.8	17.8	57.0	0.1	3.9	4.1	0.9	5.3	0.2

All GPB are dominated by silicon, aluminum and potassium stemming mainly from water glass (GEOSIL). Regarding the different Si : Al ratio, GPB mortars could be divided in three main groups:

(i) the Metaver®R based GPB mortar GP_MK1 with a high metakaolin/GEOSIL ratio displayed Si : Al = 3.7

(ii) the two Power^{TM}Pozz white based GPB mortars GP_PP and GP_PPT displayed Si : Al = 2.3

(iii) the Metaver®R based GPB mortars GP_MK2 and all GP mortars with metal additives displayed Si : Al = 1.93.

The CAC displayed the highest aluminum content of 53 wt. %, and also a calcium content of 36 wt. %. The concrete PC was dominated by calcium (64 wt. %) with a much higher content than the B6 with 19 wt. %.

Table 5: Chemical composition of the pastes and the mortar B6. The GPB pastes have a calcium-content < 1 wt. % except of GP_MK1. The GPB pastes differ mainly in the aluminum content.

Mortar/ Concrete	Paste	Na_2O	MgO	Al_2O_3	SiO_2	SO_3	K_2O	CaO	TiO_2	Fe_2O_3	Zn	Cu
GP_PP[1]												
GP_PPT	PPT	0.8	0.4	23.4	53.5	*	11.8	0.8	0.8	1.8	*	*
CAC	CAC0	0.1	0.4	52.6	5.5	*	0.2	35.7	2.3	2.5	*	*
GP_MK1	MK1	0.2	0.3	16.3	60.7	*	9.2	1.6	0.7	3.0	*	*
PC	PC0	0.3	0.9	4.0	21.8	2.4	0.3	64.3	0.2	4.3	*	*
GP_MK2	MK2	0.2	*	26.8	51.8	*	12.1	*	0.9	1.2	*	*
GP_Zn1	Zn1	*	*	26.4	51.5	*	12.2	*	0.9	1.2	0.8	*
GP_OZn1	OZn1	0.4	*	26.4	50.8	*	12.2	*	0.9	1.2	0.8	*
GP_OZn2	OZn2	0.2	*	26.0	50.9	0.5	11.7	*	1.0	1.1	1.5	*
GP_Cu1	Cu1	0.5	*	26.1	50.4	0.8	12.5	*	0.9	1.3	*	1.1
GP_Cu2	Cu2	0.4	*	25.4	51.4	1.2	11.6	*	0.8	1.2	*	1.8
B6	-	0.4	*	1.5	63.0	0.5	0.9	18.7	0.1	1.8	*	

[1]No paste available. However, the mix design for GP_PP included the paste PP0 and GEOSIL.

*Values below detection limit [b.l.d.]

A compilation of the results of the XRD patterns for the unaltered pastes and the reference concrete sample B6 is shown in the appendix A-2 (chapter 9.2). Only the main phase components are described hereafter. All GPB pastes exhibited as major phase an amorphous content of about 80 wt. % represented by the halo peak between 25 and 40 °2Theta (Figure 8). Their main crystalline phases were quartz (Qtz) and anatase (Ant). The GPB pastes with metal additives in the form of sulfates (Cu1, Cu2, Zn1) showed arcanite (K_2SO_4) as additional phase, as well as chalcocyanite ($CuSO_4$) in the case of copper. The GPB paste with the highest content of metakaolin (MK1) contained calcite (Cal) as additional phase stemming from the raw material. A representative XRD pattern of a GPB is shown in Figure 8.

CAC0, PC0 as well as the reference sample B6 contained Cal. PC0 was dominated by Qtz, Port and an amorphous phase content (C-S-H). B6 was dominated by the phases of the aggregate as Qtz and feldspar (Fsp) as well by C-S-H phases and Port. Subordinated phases in both samples were not reacted clinker phases tri calcium silicate (“alite, C_3S”) and calcium aluminate ferrite (C_4AF). The

CAC0 was dominated by calcium aluminate phases gehlenite ($C_2Al_2SiO_7$), mayenite ($C_{12}Al_{14}O_{33}$) and calcium dialuminium oxide ($CaO \cdot Al_2O_3$, "CA").

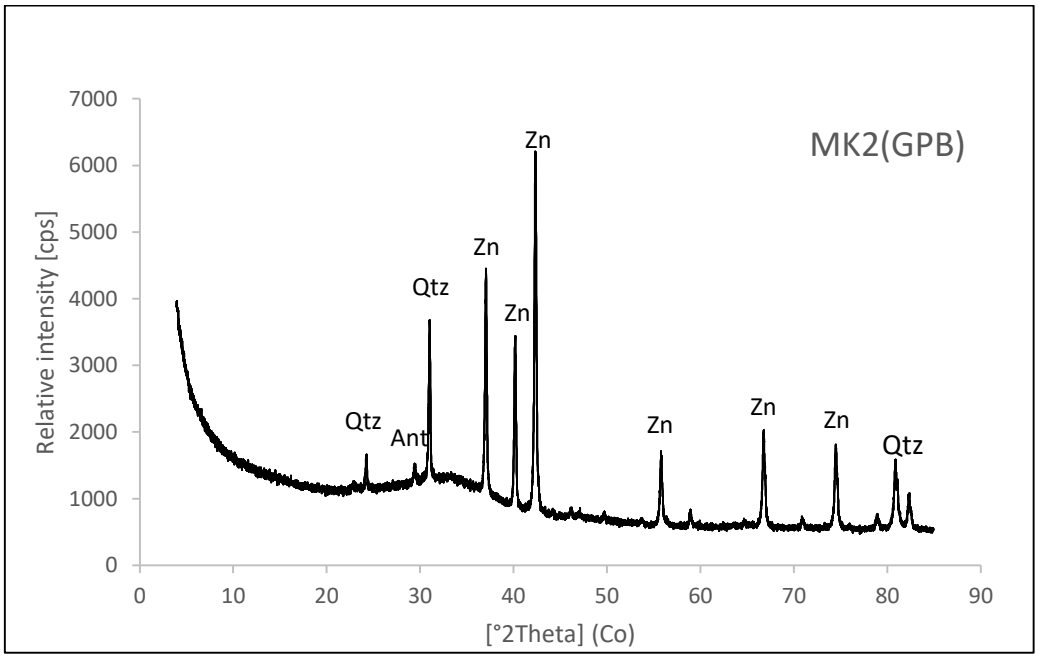

Figure 8: Typical phase content of the tested GPB pastes showing a characteristic halo peak between 25 and 40°2Theta representing the amorphous content. The crystalline phases are mainly quartz (Qtz) and anatase (Ant). The zincite peaks (Zn) arise from the additive internal standard ZnO.

Alteration

Surface pH, weight and photo documentation

A clear decrease of the surface pH of all mortars in both systems was measured, see Table 6. In system I, all samples exploited a pH decrease of > 1.4 (Figure 9). The variance of the values scattered between 0.02 and 0.97 (Table 6). The maximum decrease after 3 months was measured on the samples B6, CAC and PC. After 6 months, the pH reduction increased for GP_PPT and GP_MK1 showed the highest reduction of 4.7 from all samples. The diagram does not show the initial pH values, which were highest for the samples PC, GP_MK1, B6. Considering and comparing just the pH after 3 months, all samples showed values between 8.1 and 8.8, except of CAC with 7.8 and GP_MK1 with 9.3. The decrease rate within the second 3 months (3-6) was for all samples lower than in the first 3 months, except of GP_MK1. In system II, all samples showed a slightly lower decrease except of the samples PC, B6, GP_Cu1 and GP_Cu2. There the surface pH displayed values between 8.1 and 9.5,

except of GP_Cu1 and GP_Cu2 with 7.8 and 7.9. The results of the weight measurement are summarized in Table 7.

Table 6: Evolution of the surface pH of all measured samples after 3 and 6 months in both systems. The number of measured data is shown in brackets. For all other values, the number of measured data is 4.

Sample	$pH_{initial}$ (n)	$pH_{3\ months}$ sys I	$pH_{6\ months}$ sys I	$pH_{3months}$ sys II
GP_Zn1	9.67 ± 0.13 (4)	8.12 ± 0.25 (3)	*	8.83 ± 0.18
GP_Cu2	9.59 ± 0.15 (6)	8.09 ± 0.54 (2)	*	7.90 ± 0.02**
GP_Cu1	9.82 ± 0.07 (6)	8.40 ± 0.42	*	7.82 ± 0.02**
GP_PP	10.03 ± 0.46 (6)	8.32 ± 0.05	7.63 ± 0.70	9.39 ± 0.16
CAC	10.02 ± 0.19 (4)	7.82 ± 0.12 (3)	6.63 ± 0.72	8.40 ± 0.48
GP_PPT	10.28 ± 0.12 (4)	8.34 ± 0.56	6.78 ± 0.02	9.45 ± 0.05
GP_MK1	10.53 ± 0.19 (6)	9.25 ± 0.17	6.00 ± 0.13	9.48 ± 0.03
GP_OZn2	10.40 ± 0.18 (6)	8.63 ± 0.05 (3)	*	9.27 ± 0.22
GP_OZn1	10.50 ± 0.27 (6)	8.51 ± 0.22	*	8.91 ± 0.63
GP_MK2	10.41 ± 0.32 (6)	8.77 ± 0.22	*	9.13 ± 0.21
B6	10.96 ± 0.90 (4)	8.27 ± 0.28	7.26 ± 0.02	8.09 ± 0.70
PC	11.07 ± 0.46 (6)	8.74 ± 0.12	7.81 ± 0.97	8.18 ± 1.48

*no sampling.

** only one value measured due to a system failure.

Table 7: Evolution of the weight of all measured samples after 3 and 6 months.

	weight [g] sys I_3m		weight [g] sys II_3m		weight [g] sys I_6m	
Sample	initial	3 months	Initial	3 months	initial	6 months
GP_Zn1	250.6	253.6	248.4	246.2	*	*
GP_Cu2	244.8	245.8	254.3	250.2	*	*
GP_Cu1	256.0	258.7	255.4	253.0	*	*
GP_PP	246.9	249.5	248.6	247.9	249.7	250.0
CAC	274.0	278.8	267.0	268.9	267.6	270.4
GP_PPT	249.0	251.2	254.0	253.9	253.8	252.8
GP_MK1	255.3	255.9	250.6	249.0	250.2	248.2
GP_OZn2	255.3	257.8	250.6	249.1	*	*
GP_OZn1	251.0	253.6	253.2	252.6	*	*
GP_MK2	259.9	263.2	253.9	252.7	*	*
B6	247.2	251.4	260.0	261.4	264.0	266.3
PC	261.2	265.7	264.9	267.7	268.8	270.8

* no measurement

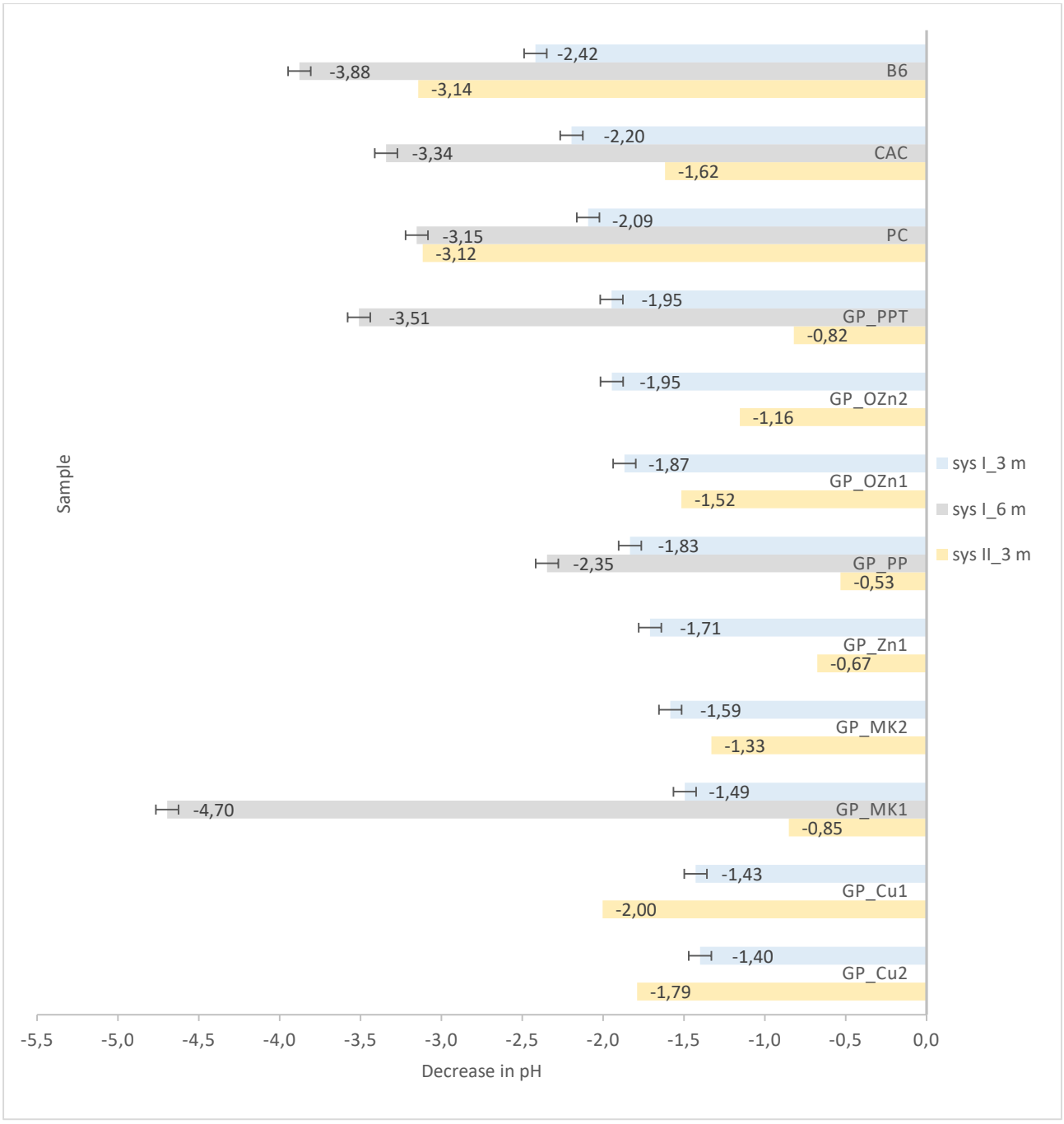

Figure 9: Trend of the surface pH of all mortar samples and the reference sample. All surface pH values show a decrease of > 1.4. Samples CAC and PC perform similar with the reference sample B6 and show the maximum pH decrease after 3 months. 3 months later, GP_MK1 exploits a decrease of 4.7 which is the highest pH change. All the other mortars tend to a reduction of the pH decrease rate within the measurement period. In system II, the two OPC-based samples exhibit the maximum decrease. With a pH decrease < 1.0, the samples GP_MK1, GP_PPT, GP_Zn1 and GP_PP display the minimum decrease, lower than all values from system I.

The weight changes for both systems are shown in Figure 10. All differences are referred to the initial weight. For system II, only one difference value exists, whereas in system I the measurement after 6 months is available.

One main trend is the weight gain of similar proportion of the two mortars (PC, CAC) and the OPC based concrete B6. After 3 months in system I, these three samples gained about 1.7 %. These three samples showed a similar trend in system II, however to a less extent. About a half of this weight gain was gone after 6 months. All GPB based mortars showed in system I a weight gain, whereas in system II a weight loss. In system I, a group of seven mortars exists, which gained about 2.2 to 3.2 g weight. GP_MK1 exhibited after 3 months only 0.62 g weight gain, as well as GP_Cu1 with only 1.00 g weight gain. There was a noticeable trend of all measured samples to lose weight within the second 3 months in system I. A totally different performance is present in system II, where all GP mortars showed a weight loss. The GP_Cu2 mortar stands out with > 4 g weight loss.

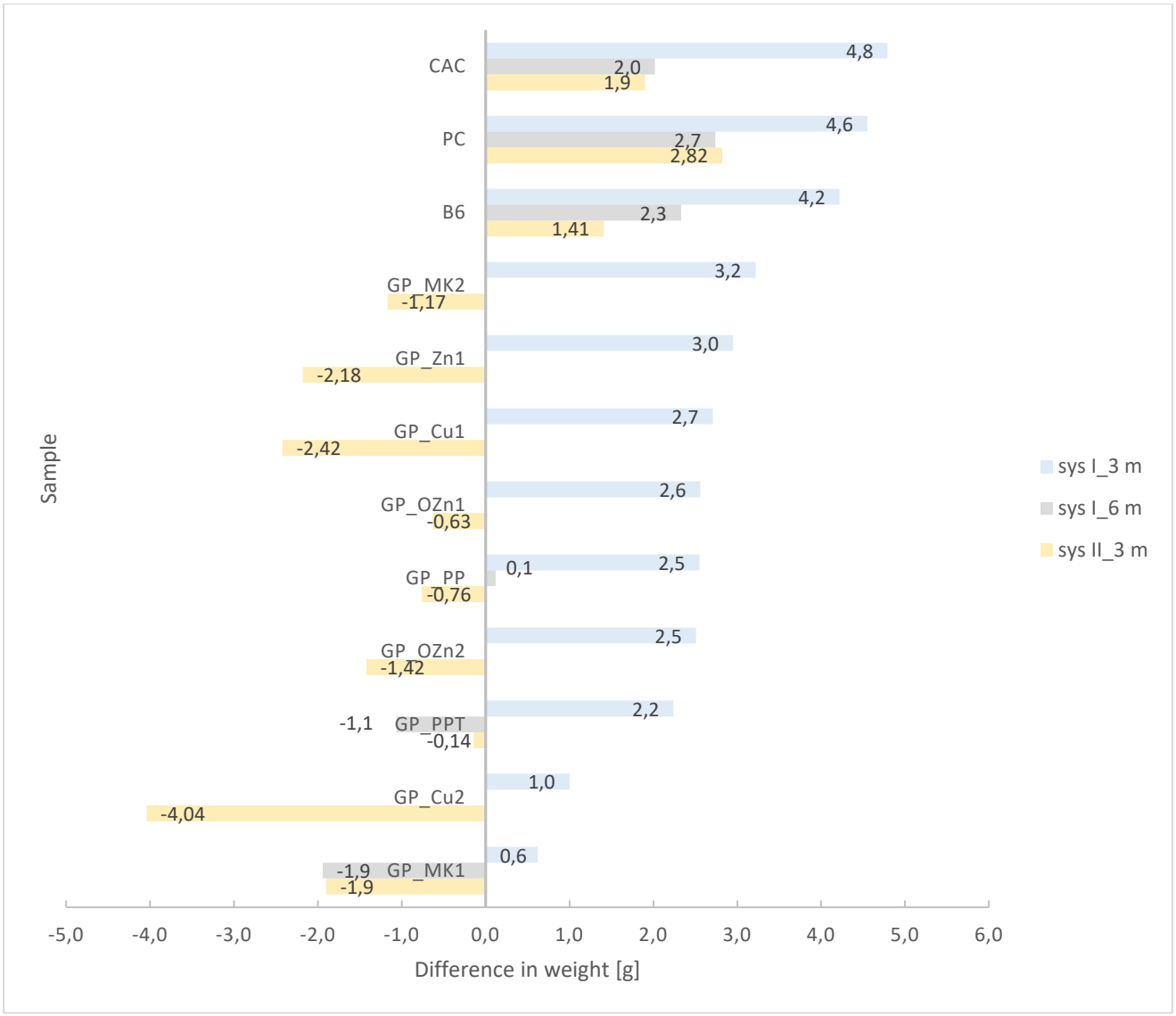

Figure 10: Trend of the weight in both systems. All differences are referred to the initial weight of a mortar sample. In system I, all samples display a weight gain after 3 months. After 6 months, samples PC, CAC and B6 have lost some of their weight gain, as well as the GP_PP mortar. GP_PPT and GP_MK1 show a similar weight loss related to the measurement after 3 months. In system II, the samples PC, CAC and B6 display a weight gain with the PC having a maximum of 2.82 g. All GPB based mortars show weight loss in different extent.

Photo documentation

Figure 11 displays the changed appearance of the sample surfaces of the two OPC based samples, the CAC and one GPB mortar after 3 and 6 months, respectively (All other surfaces are shown in the appendix chapter 9.1). The GPB mortar displayed no obvious corrosion. The OPC based samples (B6 and PC) exhibited obvious alteration of the matrix being most intense on the edge and on the matrix-aggregate boundary (white precipitation with rusty edges). The CAC mortar displayed alteration in form of a white surface precipitation which seems to be rather surficial.

Phase analysis

Table 8 displays the main results of the XRD analysis of the surface material of all samples after 3 months. The phase analysis after 6 months can be found in the Appendix A-3 (chapter 9.3). All samples, except of the CAC and the B6 in system II, exhibited elemental sulfur on the surface. All samples with calcium (PC, CAC, GP_MK1 and B6) exhibited the growth of Gp. Secondary Cal seemed to have precipitated on the surface of the samples containing the mineral already. Both mortars with copper display cuprite (Cu_2O) from the oxidation of copper sulfate ($CuSO_4$). One sample (GP_Zn1) exhibited after 3 months in system I the precipitation of arcanite (K_2SO_4).

Table 8: Qualitative XRD results of the phases removed from the sample surfaces after 3 months for both systems.

Mortar	Sulfur	Gypsum	Aragonite	Calcite	Arcanite	Cuprite
GP_PP	sys I, sys II					
GP_PPT	sys I, sys II					
CAC		sys I, sys II	sys I, sys II	sys I, sys II		
GP_MK1	sys I, sys II	sys II		sys I, sys II		
PC	sys I, sys II	sys I, sys II		sys I, sys II		
GP_MK2	sys I, sys II					
GP_Zn1	sys I, sys II				sys I, sys II	
GP_OZn1	sys I, sys II					
GP_OZn2	sys I, sys II					
GP_Cu1	sys I, sys II					sys I, sys II
GP_Cu2	sys I, sys II					sys I, sys II
B6	sys I	sys I, sys II		sys I, sys II		

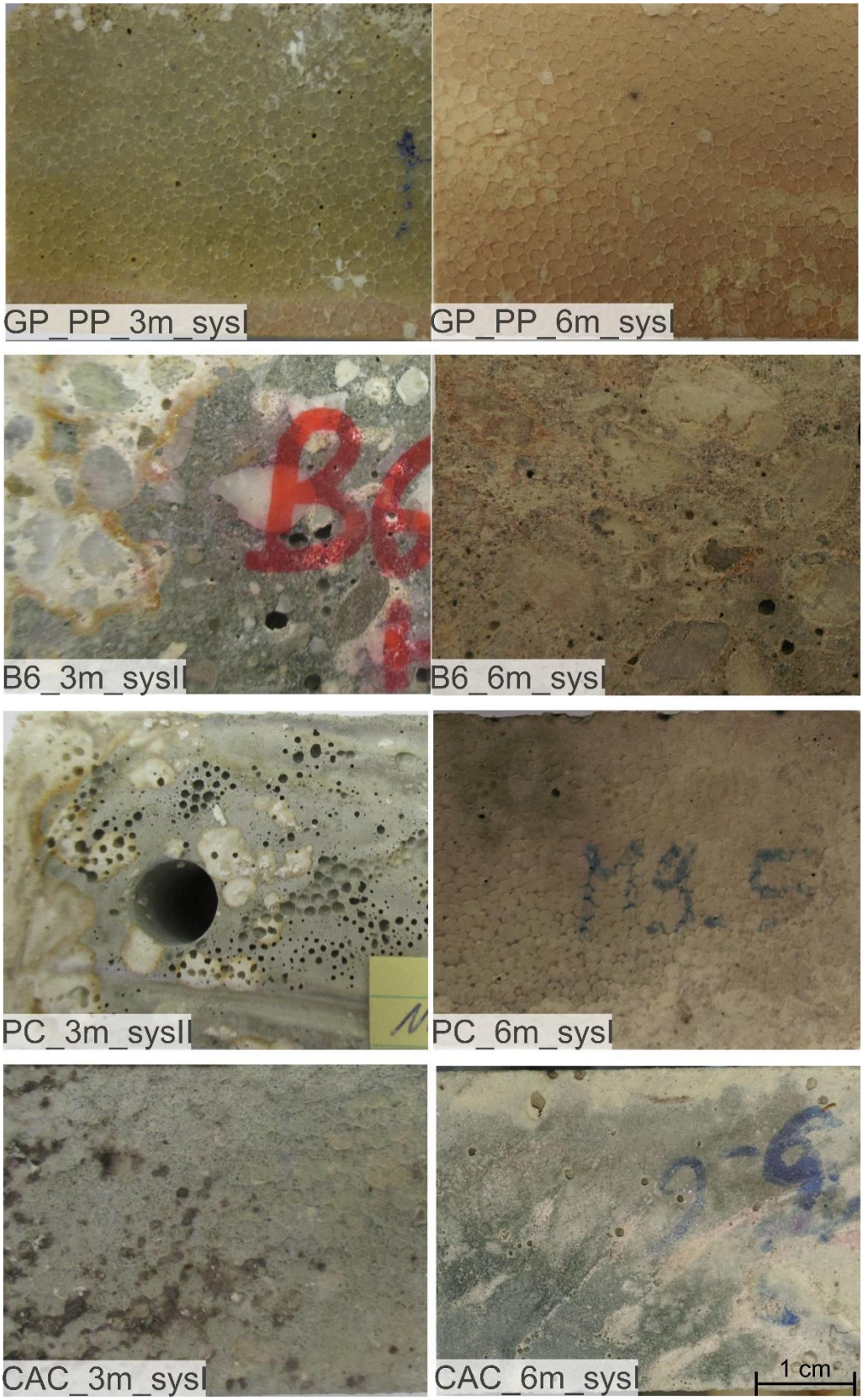

Figure 11: Visual appearance of the dried surface of the samples GP_PP, B6, PC and CAC after 3 and 6 months. The scale (bottom right) applies to each image detail.

Microscopic surface

The microscope analyses displayed alteration of all tested mortar samples to a variable extent. Results containing the under the microscope observed parameters *new solids*, *color change*, *fissures*, *bloating* are summarized for both systems in Table 9. The evaluation considers the most altered surface after 3 months in both systems. All samples displayed similar alteration characteristics in both systems, however the degree of visual alteration is higher in system II. The OPC and the CAC exhibited the most severe mineral growth (Figure 12 and Figure 13). All GPB mortar samples seemed to have less mineral growth but more physical deterioration (Figure 14 and Figure 15). A compilation of the microscopic images of all samples can be seen in the Appendix A-1 (chapter 9.1). Appendix A-1 (chapter 9.1) contains microscopic images of each sample. Only four representative examples are described in detail, containing the two samples with the most severe mineral growth (B6, CAC) and two samples (GP_MK1 and GP_PP) with the typical appearance of the GPB mortars. The largest crystals were found on the reference sample B6 (Figure 12). The translucent crystals presented an acicular habitus growing into the porosity and on the outer surface. The white bulky mineral showed a similar randomly growth but both are confined to the cement matrix. B6 also showed yellow-brown (containing Fe) corrosion margins that apparent edged the obviously deteriorated areas. A similar appearance was recognized for PC.

Table 9: Microscopic characteristics of all samples after 3 months in systems I and II.

Mortar	Color change	Mineral growth	Fissures[1]	Bloating[2]
B6_3m_sysI	White, rusty spots	xxx (amount)[3] zz (area)[4]	-	-
B6_3m_sysII	White, rusty spots	Xxx Zz	-	-
GP_PP_3m_sysI	Black spots	X Z	-	xx
GP_PP_3m_sysII	Black spots	X Z	-	xx
GP_PPT_3m_sysI	White thread-like structures	Xx Z	x	x
GP_PPT_3m_sysII	White spots	xx z	-	xx
CAC_3m_sysI	Grey-green surface	xxx z	-	-
CAC_3m_sysII	Grey-green spots	xxx z	-	-
GP_MK1_3m_sysI	White spots	x z	-	-
GP_MK1_3m_sysII	White coat	xxx z	x	-
PC_3m_sysI	Grey, small white spots	xx z	-	-
PC_3m_sysII	White spots	xxxx zz	-	x
GP_MK2_3m_sysI	White, thread-like structures	x z	-	x
GP_MK2_3m_sysII	Black spots	x z	-	-
GP_Zn1_3m_sysI	White coat	x z	-	-
GP_Zn1_3m_sysII	Black spots	x z	x	x
GP_OZn1_3m_sysI	White coat	x z	-	-
GP_OZn1_3m_sysII	Black spots	x z	x	-
GP_OZn2_3m_sysI	White structures	x z	-	-
GP_OZn2_3m_sysII	Corrosion layer with rusty edge	x z	-	-
GP_Cu1_3m_sysI	Dark grey-green with white spots	x z	-	-
GP_Cu1_3m_sysII	Dark grey-green with white spots	xx z	xx	-
GP_Cu2_3m_sysII	Dark grey-green with white spots	x z	-	-
GP_Cu2_3m_sysII	Dark grey-green with white spots	x z	xx	-

[1]x < 10 %; xx > 10 % of the investigated surface
[2]x < 10 %; xx > 10 % of the investigated surface
[3]x < 100 µm; xx > 100µm
[4]z > 0-25 %; zz >25-50 %; zzz >50-75 %; zzzz >75-100 % of the investigated surface

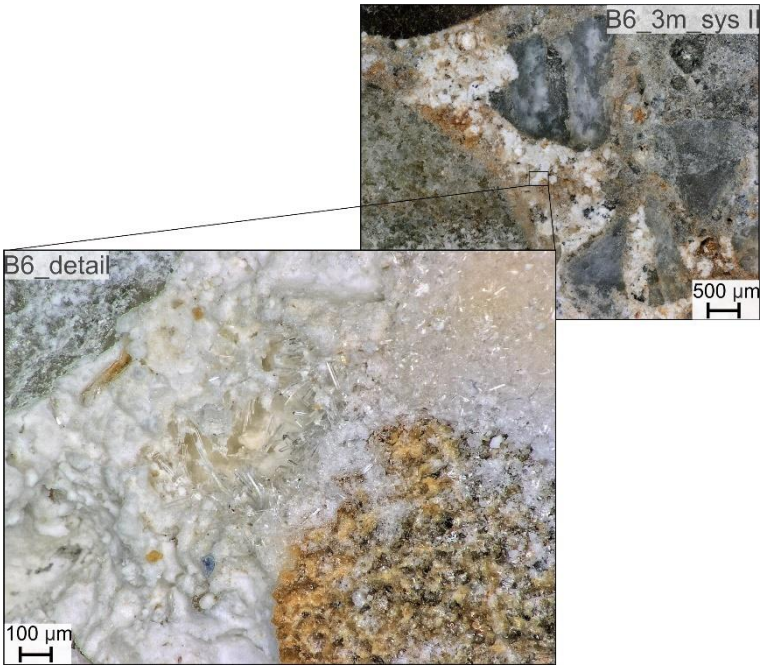

Figure 12: Microscopic figures of the surface of B6 after 3 months in system II. The surface displays the growth of new minerals of different habitus. Translucent acicular and white bulky crystals. A yellow-brown structure seems to build edges around strong deteriorated areas.

The appearance of CAC is different (Figure 13): No corrosion margins were found and the surface seemed more homogenous without large crystals grown. The surface exhibited a crystal-film of translucent to white crystals with small assemblies of yellow-greenish ones (Figure 13).

Figure 14 displays the typical appearance of the GPB mortars after 3 months. The surface was covered with a white to translucent acicular mineral. GP_MK1 exploited additionally regions with a massive white precipitate. The sample displayed also the fine, alveolate crack pattern, found on many of the GPB mortars (Table 9).

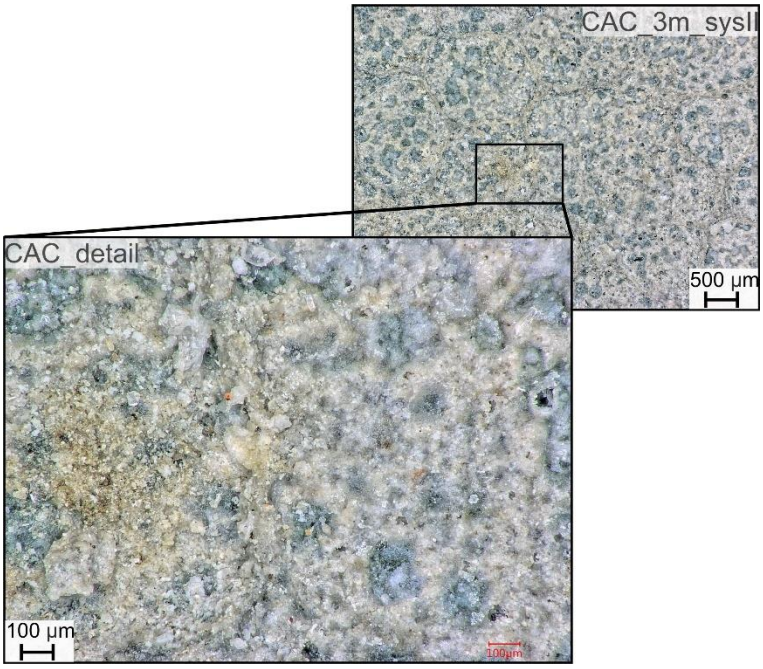

Figure 13: Microscopic details of the surface appearance of CAC mortar. The surface is covered with crystals from white to greenish color. No fissures were found.

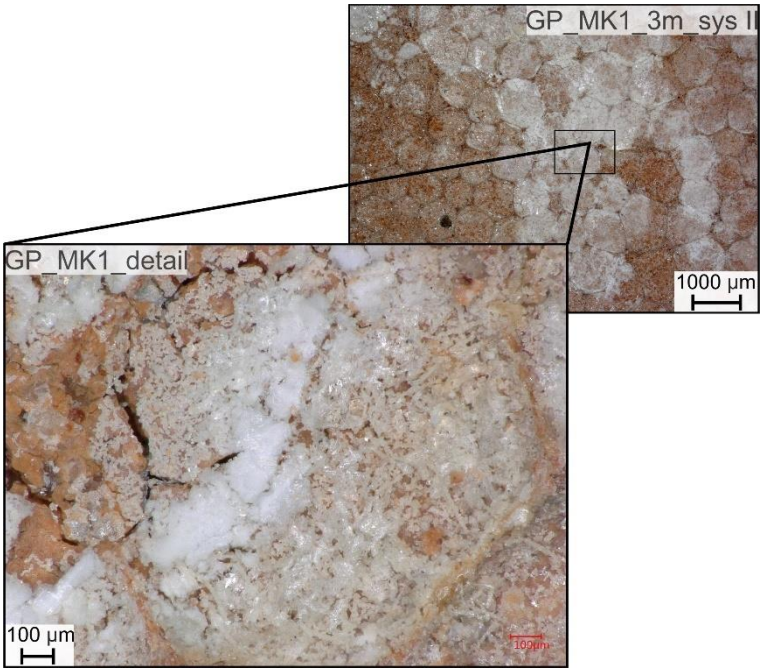

Figure 14: Microscopic picture of the surface of GP_MK1. This sample exploits all characteristics found on most of the GPB mortars to a severe extent. A coverage of small (< 100 µm), acicular, translucent to white crystals, and fine cracks. This sample displays additionally the growth of a massy white mineral.

GP_PP, performing visually better than most of the samples, displayed only a sparse growth of new minerals on the surface or in the surface porosity after 3 months. The most obvious alteration was the new surface porosity resembling a foamed-up-surface.

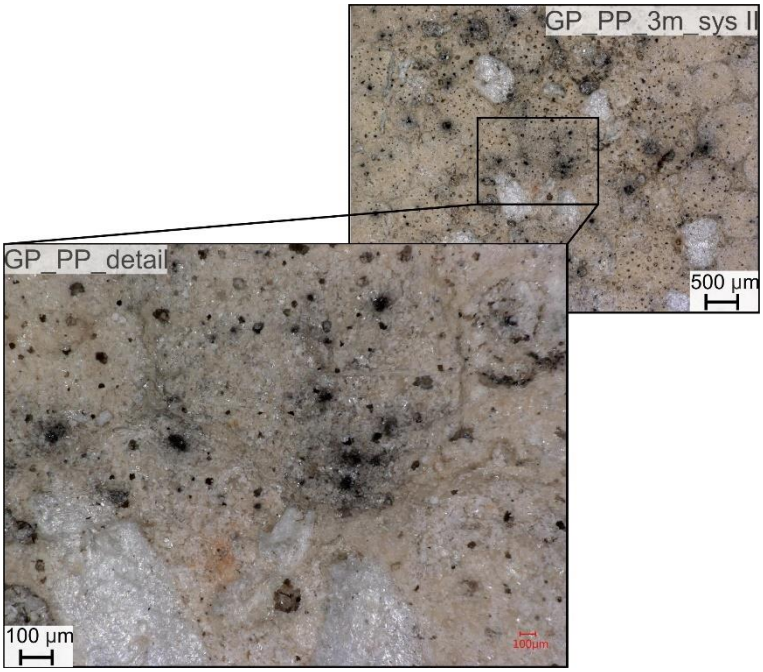

Figure 15: Microscopic picture of the surface of the PowerPozz™white-based GPB mortar. This sample exploits black spots and the formation of small pores on its surface, resembling a foamed-up-surface.

5.3 Microbiological analysis

Epifluorescence method

The relative total (death and living) cell number was determined by the epifluorescence method. The results are visualized by three pictures per sample consisting of the microscopic picture of the surface area, a picture before dying, and a picture after dying (Figure 16). All samples displayed very low (dark blue) to high (red) fluorescence. The GPB mortar with copper-sulfate ($CuSO_4$) exhibited a minimum of fluorescence in both systems (Figure 16, top). Maximum values were reached on the surface of B6 in system I (Figure 16, bottom). The average and maximum values were higher for system I than for system II. The pictures of system I are for samples GP_PP, GP_PPT, CAC and PC unfortunately not clearly to assess due to the large labelling on the surface with neon-marker. In addition, an extra chapter “Bacterial analysis” (chapter 6.3) discusses the source of the fluorescence signal.

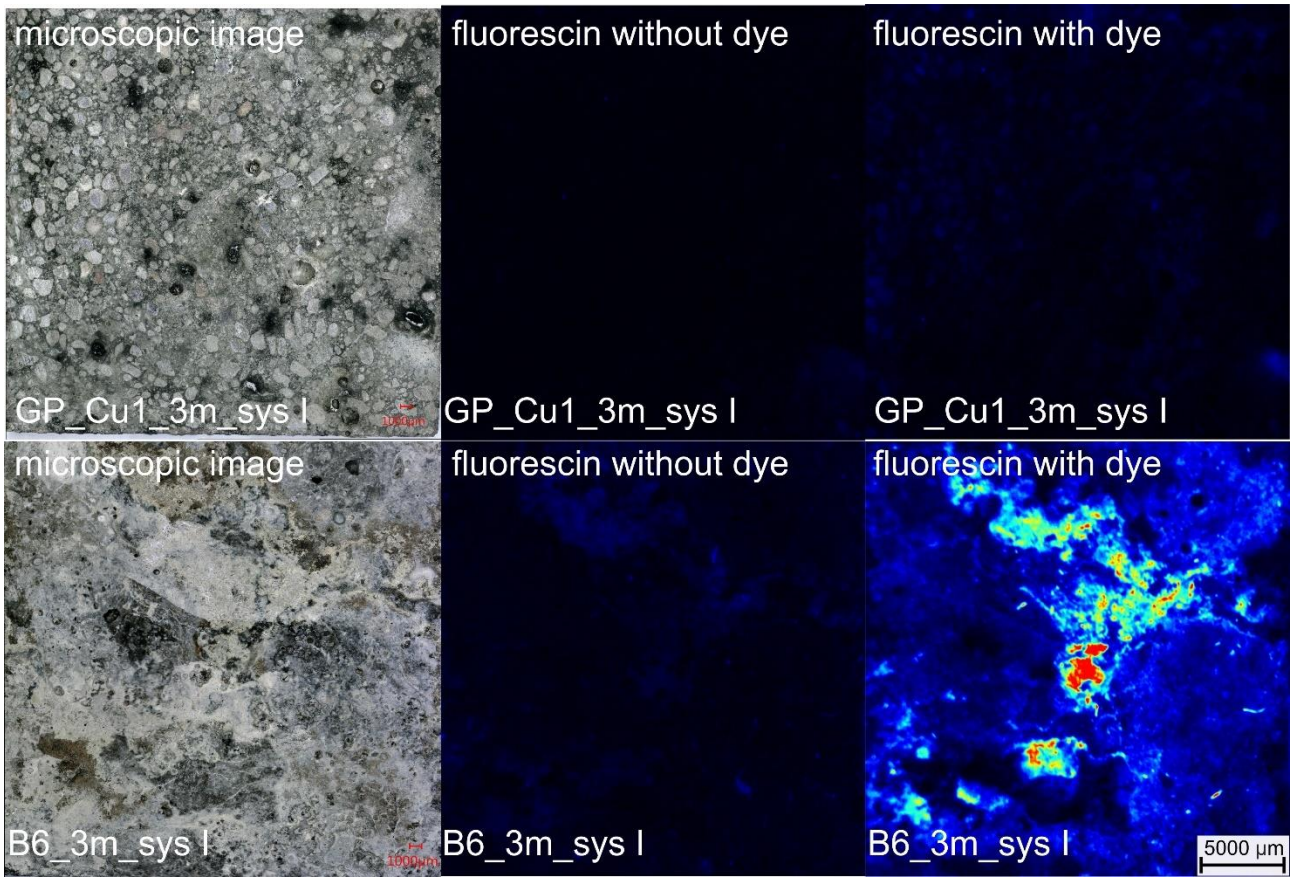

Figure 16: The pictures show for two samples, GP_Cu1 (top) and B6 (bottom) three times the same image section taken after 3 months in system I. Left a microscopic picture, the surface before dying in the middle and after dying on the right. GP_Cu1 displays least fluorescence in both systems and B6 the maximum in sys I (PC the maximum in sys II). Scale bottom right.

6. Discussion

6.1 Alteration processes in OPC based mortar/concrete and CAC based mortar

Abiotic and biotic alteration processes

In the early phase of the alteration process, the decrease in surface pH of concrete is mostly interpreted as abiotic neutralization by dissociation of hydrogen sulfide (H_2S) and carbonation [7] [64]. In this study, the tested OPC based samples (PC, B6), as well the CAC showed reaction products of carbonation, resulting from the reaction of dissolved CO_2 with the hydrated cement phases (mainly Port). This was proved by XRD pattern of sample B6 in system I showing an increased Cal peak as well as decreased Port peak (Figure 17). All other calcium containing samples (PC, CAC, GP_MK1) displayed Cal neoformation in system I. The XRD results could be supported by microscopic images of Cal assemblies (Figure 17, black box). The CAC mortar exhibited the formation of aragonite. The formation of aragonite could be associated with high supersaturation in respect to calcium carbonate formation and/or high Mg^{2+} content. In recent studies (e.g. [65] [66]) it was stated, that the type of calcium carbonate polymorph (calcite, vaterite, aragonite) forming depends on both cement type and physico-chemical conditions (e.g. diffusion rate, pH, dissolved ions) [67]. Thus, the reason for the aragonite formation on the CAC mortar is likely to be the cement type.

Additionally, the abiotic oxidation of H_2S with the pore fluids of the concrete/mortar to H_2SO_4 and polythionic acids with S^0 as intermediate [7] [68] caused a first decrease of the pH by releasing OH^- from alkaline cement phases. This can be confirmed by the presence of gypsum and elemental sulfur, common phases attributed to MICC [69], on the surface of the samples. This process is explained as the initial phase of MICC, lowering the pH by abiotic redox reactions to about 9.5. From this stage on, the colonization with various NSOB is possible [8] [9]. Indeed, bacterial analyses, presented in this thesis, showed microbial colonization. The presence of NSOB on all calcium containing samples (Master Thesis Sarah of Pycha [57]) proves the proceeding biotic oxidation of sulfur restricted to the presence of calcium. Additionally, the drop of surface pH of 7.8 after 3 months and to 6.6 after 6 months suggests that further biotic H_2SO_4 production and neutralization of alkaline cementitious phases had occurred.

Corrosion edges, in form of yellow-brown precipitates (Figure 17), were not part of the XRD analysis, but showed that the pH value in the corroded layer was sufficient low to mobilize ferrous phases that further precipitated again on the boarder to the less corroded concrete with higher pH value. This iron rust deposition is composed of various Fe^{3+} oxyhydroxides and may present an favorable environment for specific ASOB reducing Fe^{3+} to Fe^{2+} during sulfur oxidation playing a significant role in MICC [15].

Parameters influencing the alteration process

The amount of alteration phases gypsum and sulfur as products of both abiotic and biotic oxidation reactions of H_2S/Thiosulfate depends mainly on the amount of H_2S in the sewer atmosphere (pH dependent), temperature influencing the bacterial activity and the relative humidity. Since this study investigated two sewer systems, differing in both H_2S peak concentration and relative humidity, the different alteration characteristics of the samples have to be due to these parameters (and to parameters which have not been measured such as CO_2 and NH_3 gas concentrations). Though system II displayed higher H_2S peak concentrations, all samples exhibited a lower decrease in pH compared system I. This might be caused either by higher CO_2 concentrations, or by the lower relative humidity showing a higher amplitude. These intense wetting/drying cycles in system I might have led to an increased precipitation rate of acid base reaction products (similar to evaporation) and subsequently an increased diffusion rate and/or higher concentration of the acids.

This study showed, that also the type of cementitious material is crucial for how much sulfur and gypsum is formed, since the OPC based samples exhibited more gypsum than the CAC. This finding is in agreement with the observations of Herison et al. (2013) [70], who detected less sulfur on CAC. This difference is explained by Jensen et al. (2009) with catalyzed H_2S oxidation rates on specific types of cement [71]. Grandclerc et al. (2017) measured the highest H_2S adsorption rates on CEM I and relatively low ones on CAC [72]. Thus, the impact of the H_2S adsorption rate on the final alteration rate of the concrete has to be obtained. Ferrous compounds in cement are also attributed to promote the H_2S adsorption by oxidation [72]. This may be the reason for the severe gypsum formation on PC, the concrete with the highest amount of Fe_2O_3.

The presence of elemental sulfur on the concrete surface suggests that the colonization of the aerobic heterotrophic bacteria was not as intensive to consume this energy source. However, the adsorption and oxidation rate of H_2S seemed to be higher than the oxidation rate of S^0.

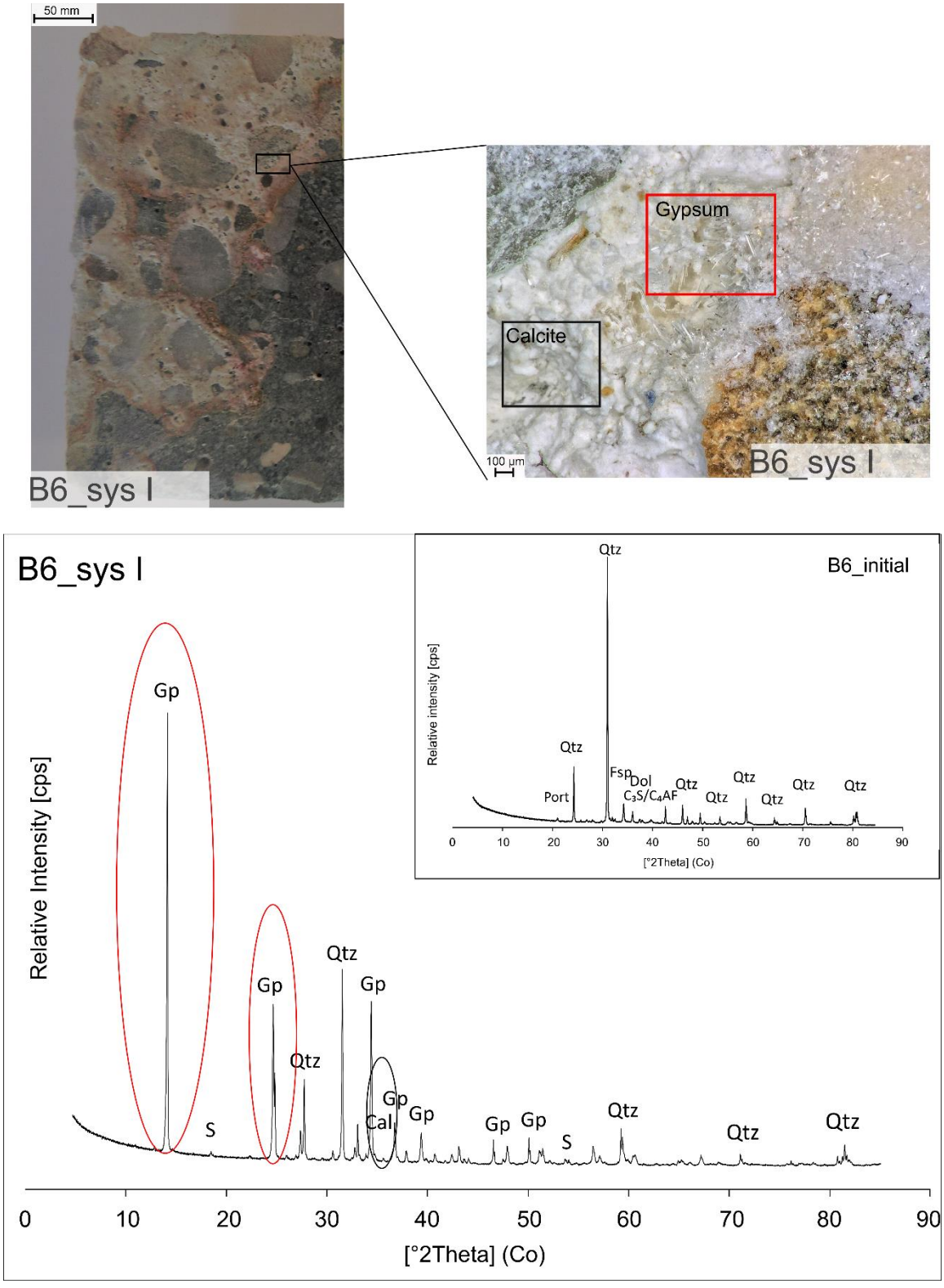

Figure 17: Dimension of the visual and chemical appearance of the OPC based sample B6 in system I. B6 in system II shows a similar pattern. Top left, the corrosion front on the edge bounded by rust margins is visible and can be correlated with the microscopic image (top right). XRD analysis of the surface precipitation (bottom left) identified the newly formed phases as mainly gypsum (Gp, outlined with red) with little calcite (Cal, outlined in black) and sulfur (S), compared with the initial bulk composition (bottom right).

6.2 Alteration processes in GPB based mortars

Alteration and leaching processes

Due to the different chemical and structural properties of the testes GPB based mortars, the alteration processes are different. The in average higher surface pH values of the GPB samples after 3 months indicate, that in the initial phase fewer acid-base reactions in form of dissolved CO_2 and poly(-thionic) acids are proceeding. The investigations of the calcium-free (< 1 wt. %) GPB mortars displayed no characteristic mineral related to carbonation (which would be potassium carbonates). Although in the XRD no carbonate phases were detected, there could still exist a relatively small amount below the detection limit (~ 1 %) of these phases. Additionally, due to the high solubility in water, the potassium carbonate might have already been dissolved - or reacted with the sulfate available in the system causing the measured drop of pH. The GP_MK1, that contained 1.6 wt. % of calcium formed calcite on the surface after 3 months in both systems as product of the reaction of dissolved CO_2 with the calcium phases. This sample displayed the highest decrease in surface pH (4.7 pH units after 6 months), caused by the replacement of Ca^{2+} by hydronium (H^+) ions. This is in accordance with Song (2005), who observed a similar behavior on fly ash based GPB under sulfuric acid attack [73]. This leaching process, replacing alkali cations by hydronium ions from reacting acids, might explain the measured decrease in surface pH of all tested GPB mortars. The impact of H_2S was verified by the mineralogical analyses of the GPB mortars after 3 and 6 months displaying elemental sulfur as the dominant newly formed phase (Figure 20). Since sulfur is the product of the partial oxidation of H_2S, it precipitates by releasing H^+ from H_2S and further incorporating it in the geopolymeric framework. By this, the alkaline K^+ is leached from the geopolymeric framework lowering the pH of the GP mortar. GP_MK1 contained gypsum after 3 months in system II as indication for the reaction of sulfuric acid with calcium phases of the mortar.

Due to the lower bacterial colonization of all GPB mortars, the biotic oxidation of H_2S was certainly less compared to the OPC and CAC based concretes. Similar findings concerning lower abiotic H_2S oxidation rates on super sulfated cementitious materials (similar to GPs) compared to CAC and OPC were recently reported from Grandclerc et al. (2017) [72]. But to what extent metabolic microbial reactions are accountable for the oxidation of H_2S in the case of the tested GPB mortars is discussed in detail in the Master thesis of Sarah Pycha [57].

The evolution of the weight of the GPB mortars for system II was characterized by weight loss, being most severe for the GPB mortars with metal sulfates (GP_Cu1, GP_Cu2, GP_Zn1). This behavior can be explained with the leaching process as previously explained. Another reason for the weight loss is probably a subordinated spalling of the material, indicated by the fissures caused by shrinkage, which were observed under the microscope. According to Davidovits (1994) [39], geopolymer cements are not prone to shrink while drying. However, this property strongly depends on the water content and porosity of the material. After 6 months in system I, GP_MK1 exhibited a highly porous surface with partly opened cracks (accompanied by a weight loss of ≈ 2 g). It is unclear, whether these structural damages were caused by internal stress due to the formation of gypsum, or present surficial fissures of drying. To reduce the high water demand during mixing of metakaolin based GPB and to achieve durable building materials, it is recommended by Xu and Van Deventer (2002) to use different alumo-silicates such as blast furnace slag (BFS) and fly ash (FA) [76]. However, both FA and BFS contain high amounts of Ca. The surface condition of the calcium-free (< 1 wt. %) GPB based samples showed fissures or blistering as well (Figure 24 and Figure 25 in chapter 7.1). Since the sulfur crystals were very small and precipitated only on the surface of the samples and not in the matrix, they were not likely to cause structural damages. Thus, the fissures might be rather surficial and originate from shallow spalling during wetting/drying cycles. In system II, where the relative humidity was more constant, the fissures are less prominent and confined to drop like spots which might be related to dripping condensed water.

In system I, all GPB mortars exhibited a weight gain after 3 months, which disappeared after 6 months (on the examined samples). Probably, it is related to the formation of sulfates on the surface, as experimentally verified on sample GP_Zn1. And residual moisture in the pore system of the materials after drying.

Parameters influencing the alteration and leaching processes

When considering the surface pH as indication, alkali leaching seemed to be more intense in system I for all GPB mortars, except of GP_Cu1/GP_Cu2. Wetting/drying cycles very likely promoting the leaching of the geopolymer matrix and pore solution. Thus, the higher drop of surface pH in system I may be the result of higher amplitudes in the humidity during wetting/drying cycles in this system causing higher diffusion rates than in system II. Additionally, the differences in the decrease of surface pH between the various tested GPs might be attributed to different structural frameworks and porosity [52]. Due to the lack of structural/porosity analyses of the tested GPB, this correlation could

not be evaluated. Song (2015) showed on SEM images of GPC leaching in acid immersion caused no structural damage after 8 weeks [74].

The diffusion rate of H_2S into the pore network is certainly lower for the GPB based mortars than for the OPC based ones and the CAC, but depends, as Bakharev (2005) [75] showed, on the porosity which is characteristic for each GPB based mortar. The microstructure of fully reacted, amorphous regions of the geopolymer matrix is composed of nano-sized (5 to 20 nm) aluminosilicate- assemblies with a nanoporosity of 3 to 10 nm [46] [47]. Thus, this parameter may be crucial to evaluate for every single sample to assess in future the entire alteration process. The porosity (and also pore size distribution) may be influenced not only by the chemical composition but also by curing procedure and degree of polymerization. Thus, these parameters are crucial for the resistance of GPC against acid attack [75]. The tested GPB displayed in the XRD analyses a halo peak between 30 and 35 ° 2Theta, which corresponds to Si-structures at a lower degree (monomers, dimers) [38]. This observation might explain the partly poor physical (crack/fissure formation and blistering) performance of the GPB samples.

The structure of the GPB mortars with metal sulfate additives is characterized by a reduced buffer capacity due to copper (or zinc) replacing potassium and additionally forming arcanite (K_2SO_4). One sample (GP_Zn1) exhibited severe efflorescence of arcanite, which indicates the mobilization of this high soluble salt (Figure 19). Thus, regarding first the evolution of the pH value, second the buffer capacity in an acid environment and third the leaching processes, the use of metal sulfates as additives seems to be unfavorable in the quantities (1.25 and 2.5 wt. % of the binder) used.

Overall, the GPB based samples performed better compared to the CAC and OPC based materials, concerning appearance, microscopic view and mineralogical composition after 3 and 6 months in both systems due to their structural properties as well as chemical composition. GPC seems to have a dense and homogenous matrix and no apparent ITZ [77] leading to low diffusion rates and low inner surface area. The choice of calcium-free binder materials is important to protect the GPC from forming expansive calcium sulfate minerals as the formation of Gp in sample GP_MK1 (with Ca) showed.

Figure 18: Severe deterioration of the sample GP_Zn1 after 3 months in system I. The mortar contains initially arcanite (K_2SO_4), which was leached out and precipitated on the surface as white-greenish efflorescence. This observation confirms, that sulfates in geopolymer cement mix design have the disadvantage to form soluble sulfates.

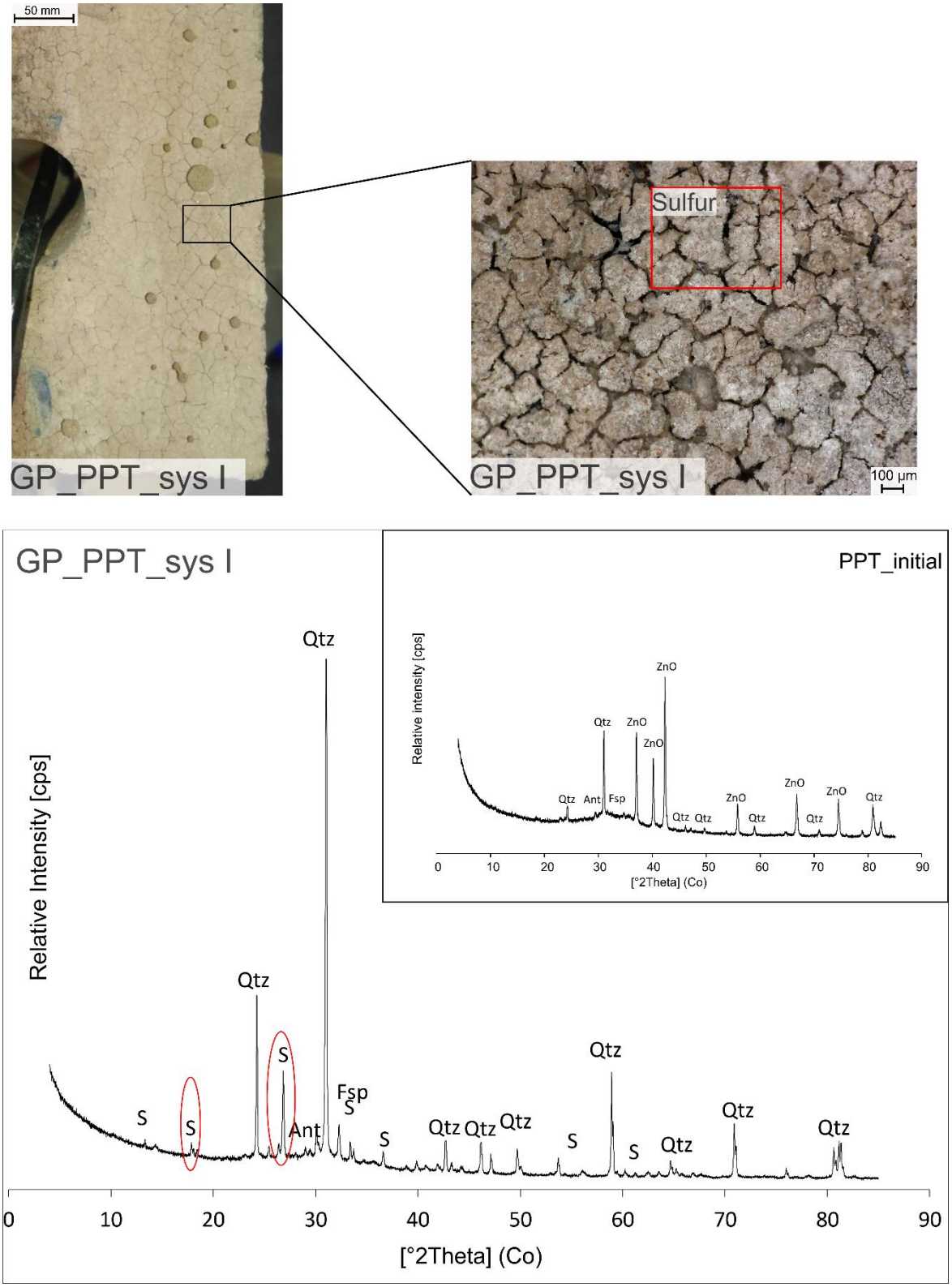

Figure 19: Compilation of the visual and chemical appearance of the PowerPozz®/TRASS based sample GP_PPT in system I. System II shows a similar pattern (not shown). Top left, the network of fissures is visible and correlated with the microscopic observation (top right). The cause of the fissures seems to be rather physical than mineralogical, since the only newly formed phase was elemental sulfur (S^0, highlighted with red).

6.3 Bacterial growth

Epifluorescence data showed a fluorescence signal on each sample except of GP_Cu2, which proves the existence of organic matter on the surface. Since for the sampling in system I the method was disturbed by the marker, only marker free results are discussed in the following. The main observation was that all GPB based mortars showed fluorescence mostly restricted to polystyrene spots as residual from the production process (Figure 20). This can be confirmed by [78], where polystyrene acted successfully as carbon source for bacterial growth. Both OPC based samples B6 and PC displayed the most severe bacterial growth on polystyrene free surface being much more intense in system I. The CAC exhibited less organic matter than the two OPC based samples. This might be caused by the higher acid neutralization capacity of $Al(OH)_3$ in CAC compared to $Ca(OH)_2$ in OPC while creating an alumina gel layer during the reaction with H_2SO_4, remaining stable down to pH 4. The precipitation of the alumina gel reduces the surface porosity and thus the percolation of H_2S as well as a biofilm adhesion [30].

The assumed antimicrobial effect of copper ions is very likely, considering the minimal fluorescence signal of GP_Cu1 and GP_Cu2 in both systems (Figure 21, system I not shown). The antimicrobial effect of Zn could not be verified since the samples with Zn displayed medium fluorescence, which was confined to polystyrene spots. Further investigations with polystyrene-free surfaces are necessary.

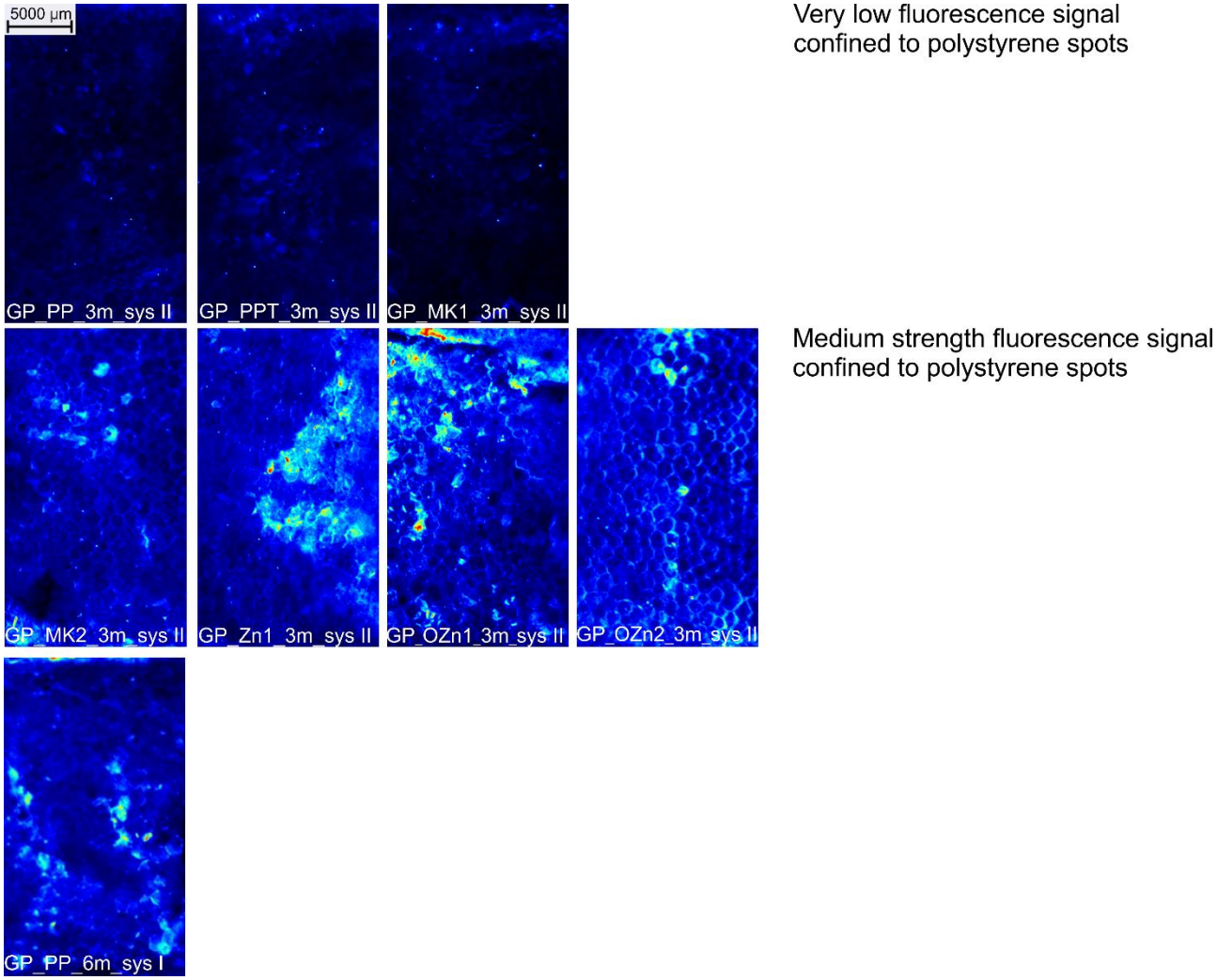

Figure 20: Epifluorescence signal after dying with fluorescein on surfaces with production-related polystyrene spots. A clear correlation of fluorescence with polystyrene was detected (high fluorescence signals confined to polystyrene-spots). Samples with Zn generally show a higher fluorescence than the others. Scale (top left) applies for each image section.

On all samples, the growth of organic matter seems not to be correlated with particular mineral assemblies, but with the unevenness of the sample surface. However, due to the overshadowing of the polystyrene spots and the marker, the results are difficult to interpret and require further investigations like DNA-analyses (further details in [57]) to determine the source of fluorescence signal, especially when restricted to polystyrene spots.

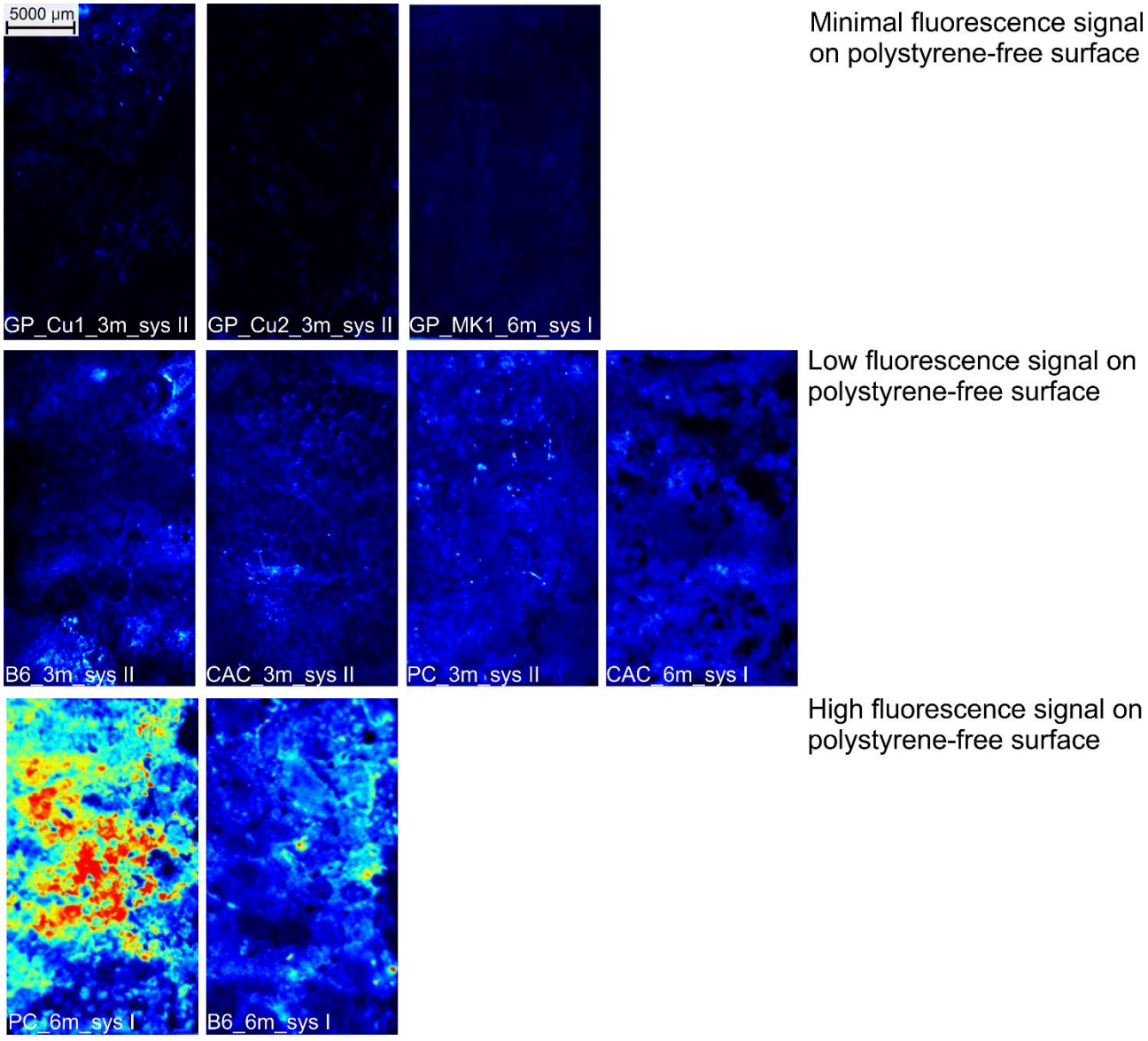

Figure 21: Epifluorescence signal after dying with fluorescein on polystyrene free surfaces. The OPC based samples display intensive bacterial growth in system I. The CAC and all GP mortars exhibit less bacterial growth especially these with copper (GP_Cu1, GP_Cu2) show an antimicrobial effect. Scale (top left) applies for each image section.

7. Conclusion and Outlook

The results after 3 and 6 months of field exposure of the materials under aggressive MICC conditions showed that the reference sample B6 together with the PC and followed by the CAC perform worst, regarding all investigated criteria, compared to the GPB based mortars.

- OPC based materials contain highly reactive C-S-H phases and Port, which react to expansive calcium sulfate salts and to carbonates when getting in contact with (poly-)thionic acids or dissolved CO_2. Since the geopolymer based mortar with calcium content displays the formation of Gps and calcite as well, the omission of calcium in the mix design seems to be crucial. However, in all GPB based mortars (including the one with calcium) no formation of any corrosion front with reduced material strength, like in the OPC based and the CAC based mortars, was observed. This is related to the difference in chemical composition and structure. The network of Si-Al bonds exhibits a higher chemical resistance in aggressive environments than C-S-H phases and Port.
- The GPB mortars displayed the highest acid buffer capacity due to free alkali cations. The metal additives tested reduced the buffer capacity by replacing alkali cations. Especially for the copper mortars, a sudden drop in the surface pH was measured. Nevertheless, no obvious correlation between the surface pH and the performance of the different types of binder could be observed. After 6 months, the surface pH of the measured GPB mortars was even lower than of the OPC based samples.
- The antimicrobial effect of copper sulfate in the GPC was verified by an obvious reduction of bacterial cell number (≈ 90 % in comparison to the other GPC) on the sample surface. Though, high concentrations of metal sulfates have turned out to destabilize the GP-structure and promote the formation of high soluble potassium sulfate.

Improved mix design and curing properties are crucial for an advanced performance of GPC. Additional investigation of material properties regarding polymerization degree and pore size distribution of GPC should be considered in future studies.

.

8. References

[1] Austrian Standards Institute, "ÖNORM B 4710-1," no. 290. Austrian Standards Institute, Vienna, pp. 1–162, 2017.

[2] M. O'Connell, C. McNally, and M. G. Richardson, "Biochemical attack on concrete in wastewater applications: A state of the art review," *Cem. Concr. Compos.*, vol. 32, no. 7, pp. 479–485, 2010.

[3] Hvitved-Jacobsen, T, J. Vollertsen, C. Yongsiri, and a H. Nielsen, "Sewer microbial processes , emissions and impacts," *Sewers Process networks*, p. 13, 2002.

[4] A. Eštokova, V. O. Harbuláková, A. Luptáková, and N. Števulová, "Study of the deterioration of concrete influenced by biogenic sulphate attack," *Procedia Eng.*, vol. 42, no. August, pp. 1731–1738, 2012.

[5] S.-H. Gao, J. Y. Ho, L. Fan, D. J. Richardson, Z. Yuan, and P. L. Bond, "Antimicrobial effects of free nitrous acid on Desulfovibrio vulgaris : implications for sulfide induced concrete corrosion," *Appl. Environ. Microbiol.*, vol. 82, no. 18, pp. 5563–5575, 2016.

[6] M. Holmer, H. Hasler-sheetal, M. Holmer, and H. Hasler-sheetal, "Sulfide intrusion in seagrasses assessed by stable sulfur isotopes-A synthesis of current results Sulfide intrusion in seagrasses assessed by stable sulfur isotopes — a synthesis of current results," *Front. Mar. Sci.*, vol. 1, pp. 1–12, 2014.

[7] T. Wells, R. E. Melchers, and P. Bond, "Factors involved in the long term corrosion of concrete sewers," *49th Annu. Conf. Australas. Corros. Assoc.*, pp. 345–356, 2009.

[8] B. R. L. Islander, J. S. Devinny, A. Member, F. Mansfeld, A. Postyn, and H. Shih, "Microbial ecology of crown corrosion in sewers," *J. Environ. Eng.*, vol. 117, no. 6, pp. 751–770, 1992.

[9] K. Cho and T. Mori, "A newly isolated fungus participates in the corrosion of concrete sewer pipes," *Water Sci. Technol.*, vol. 31, no. 7, pp. 263–271, 1995.

[10] D. Nica, J. L. Davis, L. Kirby, G. Zuo, and D. J. Roberts, "Isolation and characterization of microorganisms involved in the biodeterioration of concrete in sewers," *Int. Biodeterior. Biodegradation*, vol. 46, no. 1, pp. 61–68, Jul. 2000.

[11] X. Li, U. Kappler, G. Jiang, and P. L. Bond, "The ecology of acidophilic microorganisms in the corroding concrete sewer environment," *Front. Microbiol.*, vol. 8, pp. 1–16, 2017.

[12] G. Jiang, M. Zhou, T. H. Chiu, X. Sun, J. Keller, and P. L. Bond, "Wastewater-Enhanced Microbial Corrosion of Concrete Sewers," *Environ. Sci. Technol.*, vol. 50, no. 15, pp. 8084–

8092, 2016.

[13] A. L. Ling, C. E. Robertson, J. K. Harris, D. N. Frank, C. V. Kotter, M. J. Stevens, N. R. Pace, and M. T. Hernandez, "High-resolution microbial community succession of microbially induced concrete corrosion in working sanitary manholes," *PLoS One*, vol. 10, no. 3, pp. 1–12, 2015.

[14] A. Vollpracht, B. Lothenbach, R. Snellings, and J. Haufe, "The pore solution of blended cements : a review," *Mater. Struct.*, vol. 49, no. 8, pp. 3341–3367, 2016.

[15] C. Grengg and F. Mittermayr, "The decisive role of acidophilic bacteria in concrete sewer networks: A new model for fast progressing microbial concrete corrosion." (in press)

[16] K. L. Scrivener, A. K. Crumbie, and P. Laugesen, "The Interfacial Transition Zone (ITZ) between Cement Paste and Aggregate in Concrete," *Interface Sci.*, vol. 12, no. 4, pp. 411–421, 2004.

[17] C. Grengg, F. Mittermayr, A. Baldermann, M. E. Böttcher, A. Leis, G. Koraimann, P. Grunert, and M. Dietzel, "Microbiologically induced concrete corrosion: A case study from a combined sewer network," *Cem. Concr. Res.*, vol. 77, pp. 16–25, 2015.

[18] T. Mori, T. Nonaka, K. Tazaki, and Et.al, "Interactions of nutrients, moisture and pH on microbial corrosion of concrete sewer pipes," *Water Res.*, vol. 26, no. 1, pp. 29–37, Jan. 1992.

[19] T. Mori, M. Koga, Y. Hikosaka, T. Nonaka, F. Mishina, Y. Sakai, and J. Koizumi, "Microbial Corrosion of Concrete Sewer Pipes, H2S Production from Sediments and Determination of Corrosion Rate," *Water Sci. Technol.*, vol. 23, no. 7–9, pp. 1275–1282, Apr. 1991.

[20] N. De Belie, J. Monteny, A. Beeldens, E. Vincke, D. Van Gemert, and W. Verstraete, "Experimental research and prediction of the effect of chemical and biogenic sulfuric acid on different types of commercially produced concrete sewer pipes," *Cem. Concr. Res.*, vol. 34, no. 12, pp. 2223–2236, 2004.

[21] C. D. Parker, "The corrosion of concrete 1. The isolation of a species of bacterium associated with the corrosion of concrete exposed to atmospheres containing hydrogen sulphides," *Aust. J. Exp. Biol. Med. Sci.*, vol. 23, no. 2, pp. 81–90, 1945.

[22] S. Okabe, M. Odagiri, T. Ito, and H. Satoh, "Succession of sulfur-oxidizing bacteria in the microbial community on corroding concrete in sewer systems.," *Appl. Environ. Microbiol.*, vol. 73, no. 3, pp. 971–80, Feb. 2007.

[23] M. C. G. Juenger, F. Winnefeld, J. L. Provis, and J. H. Ideker, "Advances in alternative cementitious binders," *Cem. Concr. Res.*, vol. 41, no. 12, pp. 1232–1243, 2011.

[24] J. Bied, *Recherches industrielles sur les chaux, ciments et mortiers.* Paris, 1926.

[25] T. Delibas, Ö. Kirca, and I. Ö. Yaman, “The usage of calcium aluminate cement in Terrazzo type floor tyles,” in *Calcium Aluminates: Proceedings of the International Conference*, 2014, pp. 479–487.

[26] H. Yi and M. D. A. Thomas, “The performance of CAC concrete in an aggressive marine environment,” in *Calcium Aluminates: Proceedings of the International Conference*, 2014, pp. 556–569.

[27] A. Govin, I. Albuquerque, and P. Grosseau, “Development of an accelerated test of fungal biodeterioration: Application to calcium aluminate cements,” in *Calcium Aluminate Cements: Proceedings of the Centenary Conference*, 2014, pp. 511–522.

[28] A. M. Goyns and M. G. Alexander, “Performance of various concretes in the Virginia experimental sewer over 20 years,” in *Calcium Aluminates: Proceedings of the International Conference*, 2014, pp. 573–584.

[29] K. L. Scrivener and A. Capmas, “Calcium Aluminate Cements 2001,” in *Lea’s Chemistry of Cement and Concrete*, Fourth Edi., P. C. Hewlett, Ed. Elsevier Ltd., 2001, pp. 713–782.

[30] J. Herisson, E. Van Hullebusch, T. Chaussadent, and M. Guéguen-Minerbe, “Biogenic corrosion mechanism: Study of parameters explaining calcium aluminate cement durability,” in *Calcium Aluminate Cements: Proceedings of the International Conference*, 2014, pp. 633–644.

[31] P. Garcidueñas, Rogelio Cervantes, “Microbial interactions with aluminium,” *Biometals*, vol. 9, no. 3, pp. 311–316, 1996.

[32] J. G. Joshi, “Aluminum, a neurotoxin which affects diverse metabolic reactions,” *Biofactors*, vol. 2, no. 3, p. 163—169, 1990.

[33] N. Yoshida, Y. Murooka, and K. Ogawa, “Heavy metal particle resistance in Thiobacillus intermedius 13-1 isolated from corroded concrete,” *J. Ferment. Bioeng.*, vol. 85, no. 6, pp. 630–633, Jan. 1998.

[34] J. Fischer, A. Quentmeier, S. Gansel, V. Sabados, and C. G. Friedrich, “Inducible aluminum resistance of Acidiphilium cryptum and aluminum tolerance of other acidophilic bacteria,” *Arch. Microbiol.*, vol. 178, no. 6, pp. 554–558, 2002.

[35] N. Olsen, “German Patent 600,” 1934.

[36] A. O. Purdon, “L’action des alcalis sur laitier de haut-founeau,” *J. la Société des Ind. Chim.*, vol. 59, pp. 191–202, 1940.

[37] W. E. Station, “Tests of Trief Cement and Laboratory-ground, Water-quenched, Blast-furnace Slag Cement,” 1953.

[38] J. Davidovits, *Geopolymer: Chemistry and Applications*, vol. 4. 2015.

[39] J. Davidovits, “Properties of Geopolymer Cements,” in *Alkaline Cements and Concretes: Proceedings of the First International Conference.*, 1994, pp. 131–149.

[40] J. Davidovits, “Geopolymers - Inorganic polymeric new materials,” *J. Therm. Anal.*, vol. 37, no. 8, pp. 1633–1656, 1991.

[41] R. M. Barrer, L. Hinds, and E. A. White, “The hydrothermal chemistry of silicates. Part III. Reactions of analcite and leucite,” *J. Chem. Soc.*, pp. 1466–1475, 1953.

[42] J. Davidovits, “Geopolymer Cement, a review,” *Geopolymer Inst. Libr.*, pp. 1–11, 2013.

[43] J. Davidovits and J.-J. Legrand, “French Patent FR 2,324,427,” 1974.

[44] J. Davidovits and J.-J. Legrand, “US Patent 4,028,454.”

[45] P. Duxson and J. S. J. Van Deventer, “17 – Commercialization of geopolymers for construction – opportunities and obstacles,” in *Geopolymers: Structures, Processing, Properties and Industrial Applications*, 1st ed., J. L. Provis and J. S. J. van Deventer, Eds. 2009, pp. 379–400.

[46] W. M. Kriven, J. L. Bell, and M. Gordon, “Microstructure and Microchemistry of Fully-Reacted Geopolymers and Geopolymer Matric Composites,” *Ceram. Trans.*, vol. 260, pp. 227–250, 2016.

[47] J. Sindhunate, J. S. J. van Deventer, G. C. Lukey, and H. Xu, “Effect of Curing Temperature and Silicate Concentration on Fly-Ash-Based Geopolymerization,” *Ind. Eng. Chem. Res.*, vol. 45, no. 10, pp. 3559–3568, 2006.

[48] J. L. Provis and C. A. Rees, “Geopolymer synthesis kinetics,” in *Geopolymers*, 1st ed., J. L. Provis and J. S. J. van Deventer, Eds. 2009, pp. 118–136.

[49] J. L. Provis, G. C. Lukey, and J. S. J. van Deventer, “Do Geopolymers Actually Contain Nanocrystalline Zeolites? A Reexamination of Existing Results,” *Chem. Mater.*, vol. 17, no. 12, pp. 3075–3085, Jun. 2005.

[50] P. J. Davidovits, “30 Years of Successes and Failures in Geopolymer Applications . Market Trends and Potential Breakthroughs .,” *Geopolymer 2002 Conf.*, pp. 1–16, 2002.

[51] J. S. J. Van Deventer, J. L. Provis, and P. Duxson, “Technical and commercial progress in the adoption of geopolymer cement,” *Miner. Eng.*, vol. 29, pp. 89–104, 2012.

[52] N. Ukrainczyk, O. Vogt, and E. A. B. Koenders, “Reactive Transport Numerical Model for Durability of Geopolymer Materials,” *Adv. Chem. Eng. Sci.*, vol. 6, no. 4, pp. 355–363, 2016.

[53] M. Cyr and R. Pouhet, “Carbonation in the pore solution of metakaolin-based geopolymer,” *Cem. Concr. Res.*, vol. 88, pp. 227–235, 2016.

[54] E. Najafi Kani, A. Allahverdi, and J. L. Provis, “Efflorescence control in geopolymer binders based on natural pozzolan,” *Cem. Concr. Compos.*, vol. 34, no. 1, pp. 25–33, 2012.

[55] R. Suchý, J. Pořízka, J. Wasserbauer, and L. Kalina, “Reduction of Efflorescence in the Alkali Activated Systems,” *Adv. Mater. Res.*, vol. 1000, pp. 318–321, 2014.

[56] J. L. Provis, P. Duxson, and J. S. J. van Deventer, “The role of particle technology in developing sustainable construction materials,” *Adv. Powder Technol.*, vol. 21, no. 1, pp. 2–7, 2010.

[57] S. Pycha, “Biogenic sulfur corrosion in sewage systems,” (in press).

[58] K. Delgado, R. Quijada, R. Palma, and H. Palza, “Polypropylene with embedded copper metal or copper oxide nanoparticles as a novel plastic antimicrobial agent,” *Lett. Appl. Microbiol.*, vol. 53, no. 1, pp. 50–54, 2011.

[59] M. Dopson, C. Baker-Austin, P. R. Koppineedi, and P. L. Bond, “Growth in sulfidic mineral environments: Metal resistance mechanisms in acidophilic micro-organisms,” *Microbiology*, vol. 149, no. 8, pp. 1959–1970, 2003.

[60] K. R. Raghupathi, R. T. Koodali, and A. C. Manna, “Size-Dependent Bacterial Growth Inhibition and Mechanism of Antibacterial Activity of Zinc Oxide Nanoparticles,” *Langmuir*, vol. 27, no. 7, pp. 4020–4028, Apr. 2011.

[61] C. Huber, I. Klimant, C. Krause, and O. S. Wolfbeis, “Dual lifetime referencing as applied to a chloride optical sensor,” *Anal. Chem.*, vol. 73, no. 9, pp. 2097–2103, 2001.

[62] B. Müller, “Luminescent pH-sensitive Nanoparticles for the Application in Microfluidic Systems,” 2015.

[63] D. L. Bish and J. Reynolds, R.C., “Sample preparation for X-ray diffraction,” *Mod. Powder Diffraction.Reviews Mineral.*, vol. 20, pp. 73–99, 1989.

[64] H. S. Jensen, J. L. Nielsen, K. Bester, A. H. Nielsen, T. Hvitved-Jacobsen, and J. Vollertsen, “Growth kinetics of hydrogen sulfide oxidizing bacteria in corroded concrete from sewers,” *J. Hazard. Mater.*, vol. 189, no. 3, pp. 685–691, 2011.

[65] W. Ashraf, “Carbonation of cement-based materials: Challenges and opportunities,” *Constr.*

Build. Mater., vol. 120, no. November, pp. 558–570, 2016.

[66] S. Goñi, M. T. Gaztañaga, and A. Guerrero, “Role of Cement Type on Carbonation Attack,” *J. Mater. Res.*, vol. 17, no. 7, pp. 1834–1842, 2002.

[67] G. W. Groves, D. I. Rodway, and I. G. Richardson, “The carbonation of hardened cement pastes,” *Adv. Cem. Res.*, vol. 3, no. 11, pp. 117–125, 1990.

[68] J. Vollertsen, A. H. Nielsen, H. S. Jensen, T. Wium-Andersen, and T. Hvitved-Jacobsen, “Corrosion of concrete sewers - The kinetics of hydrogen sulfide oxidation,” *Sci. Total Environ.*, vol. 394, no. 1, pp. 162–170, 2008.

[69] A. P. Joseph, J. Keller, H. Bustamante, and P. L. Bond, “Surface neutralization and H2S oxidation at early stages of sewer corrosion: Influence of temperature, relative humidity and H2S concentration,” *Water Res.*, vol. 46, no. 13, pp. 4235–4245, 2012.

[70] J. Herisson, E. D. van Hullebusch, M. Moletta-Denat, P. Taquet, and T. Chaussadent, “Toward an accelerated biodeterioration test to understand the behavior of Portland and calcium aluminate cementitious materials in sewer networks,” *Int. Biodeterior. Biodegradation*, vol. 84, pp. 236–243, 2013.

[71] H. S. Jensen, A. H. Nielsen, T. Hvitved-Jacobsen, and J. Vollertsen, “Modeling of Hydrogen Sulfide Oxidation in Concrete Corrosion Products from Sewer Pipes,” *Water Environ. Res.*, vol. 81, no. 4, pp. 365–373, 2009.

[72] A. Grandclerc, M. Guéguen-Minerbe, I. Nour, P. Dangla, and T. Chaussadent, “Impact of cement composition on the adsorption of hydrogen sulphide and its subsequent oxidation onto cementitious material surfaces,” *Constr. Build. Mater.*, vol. 152, pp. 576–586, 2017.

[73] N. Atiq, S. Ahmed, M. Ali, and S. Andleeb, “Isolation and identification of polystyrene biodegrading bacteria from soil,” *African J. Microbiol. Res.*, vol. 4, no. November 2006, pp. 1537–1541, 2010.

9. Appendix

9.1 Appendix A-1

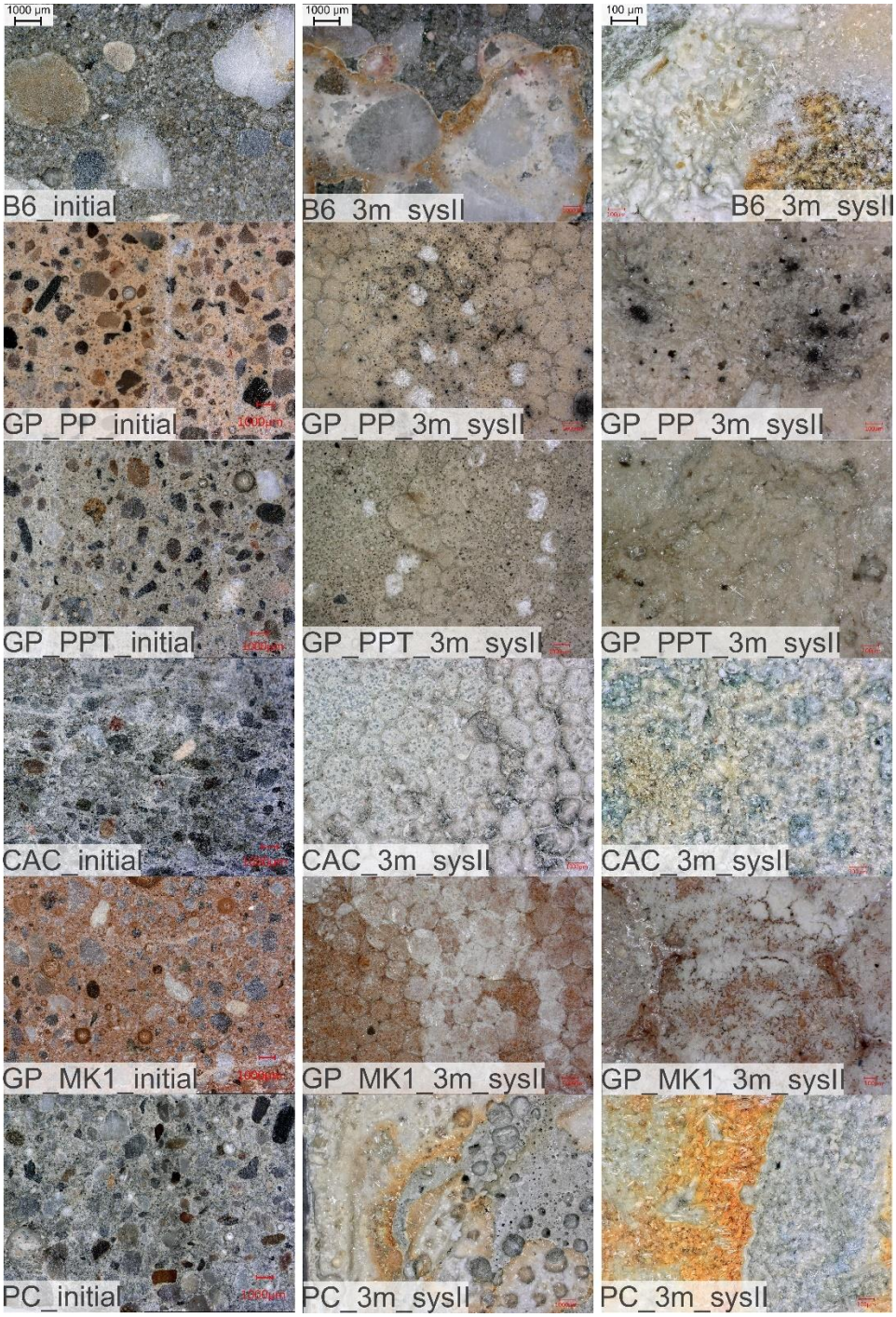

Figure 22: Microscopic images of samples in their initial state (rough-cut) and after 3 months in system II. The image on the left shows the most detailed picture with 200x magnification. Scale applies for each row of image sections.

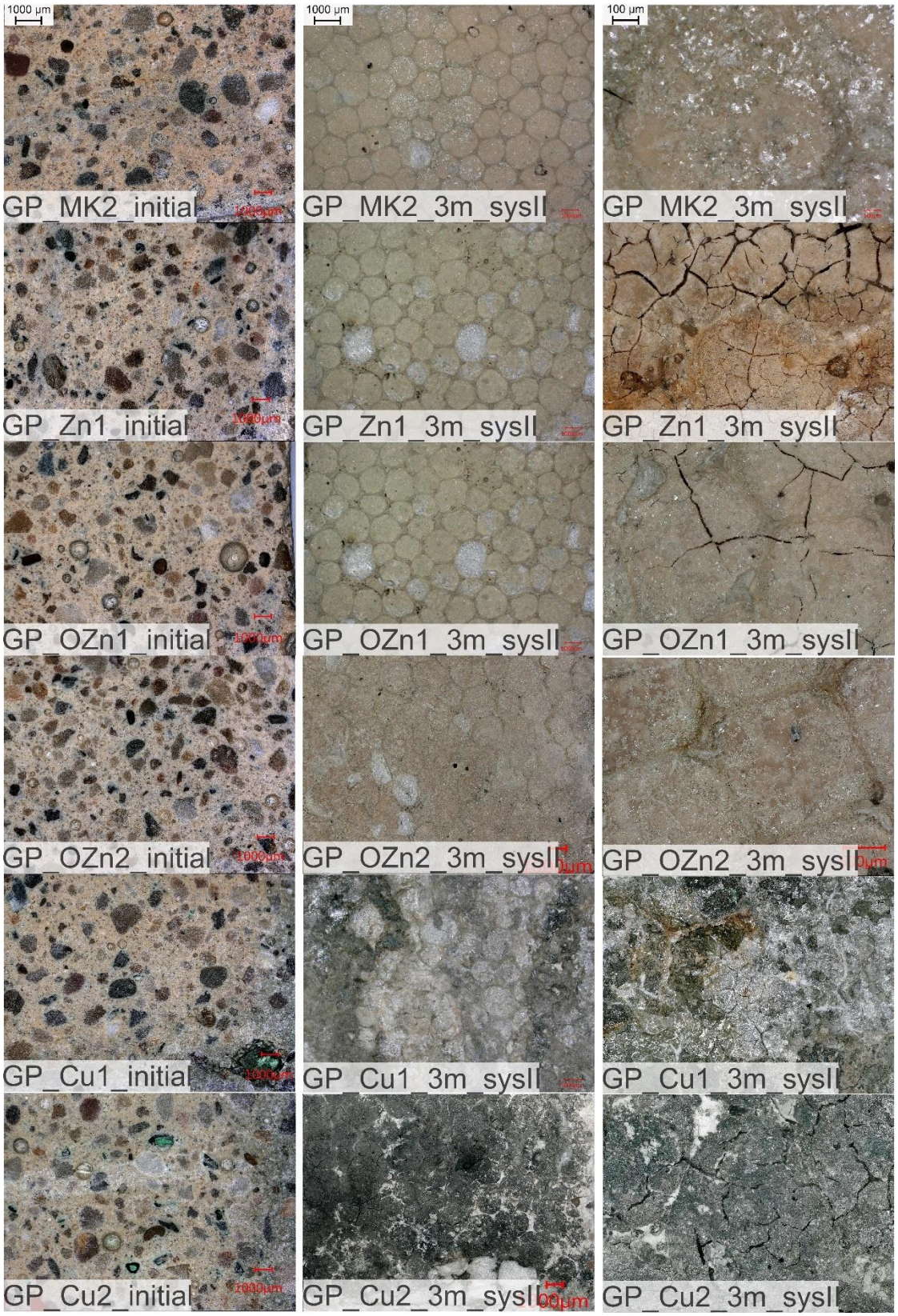

Figure 23: Microscopic images of the GPB mortar GP_MK2 without and with additives in their initial state (rough-cut) and after 3 months in system II. The image on the left shows the most detailed picture with 200x magnification.

9.2 Appendix A-2

Table 10: Initial crystalline phase content of the used raw materials, all paste samples and the tested concrete B6. In all materials, an amorphous content of different extent was measured.

	B6	PC0	CAC0	PP0	TRASS	MW0	MWM	PT30	GP_MK2	GP_ Zn1	GP_ OZn1	GP_ OZn2	GP_ Cu1	GP_ Cu2
Analcime					x									
Anatase				x		x	x	x	x	x	x	x	x	x
Arcanite										x			x	x
Augite					x									
Ferrite C_4AF-	x	x												
Calcite	x	x	x			x	x							
Chabazite					x									
Chalcocyanite													x	x
Chamosite					x									
Dolomite	x													
Fsp-group	x			x				x						
Gehlenite			x											
Alite C_3S	x	x												
Hematite						x								
Illite						x								
Belite β-C_2S		x												
Leucite					x									
Mayenite			x											
Microcline														
Muscovite					x									
Portlandite	x	x	x											
Quartz	x	x	x	x	x	x	x	x	x	x	x	x	x	x

9.3 Appendix A-3

Table 11: Phase content of the surface precipitation after 6 months in system II for the six tested samples.

Mortar	Sulfur	Gypsum	Calcite
GP_PP	x		
GP_PPT	x		
CAC	x	x	x
GP_MK1	x	x	
PC	x	x	x
B6	x	x	x